HHS Public Access

Author manuscript

Neuroscience. Author manuscript; available in PMC 2021 August 01.

Published in final edited form as:

Neuroscience. 2020 August 01; 440: 299–315. doi:10.1016/j.neuroscience.2020.04.024.

Identification of novel targets of RBM5 in the healthy and injured brain.

Travis C. Jackson[1,2], **Keri Janesko-Feldman**[3], **Kiersten Gorse**[1,2], **Vincent A. Vagni**[3], **Edwin K. Jackson**[4], **Patrick M. Kochanek**[3]

[1]Primary Laboratory, University of South Florida, Morsani College of Medicine, USF Health Heart Institute, MDD 0742, 560 Channelside Dr, Tampa FL, 33602

[2]University of South Florida, Morsani College of Medicine, Department of Molecular Pharmacology & Physiology, 12901 Bruce B Downs BLDV, Tampa FL, 33612-4799

[3]Safar Center for Resuscitation Research, UPMC Children's Hospital of Pittsburgh, Rangos Research Center – 6th floor, Pittsburgh, PA 15224

[4]University of Pittsburgh School of Medicine, Department of Pharmacology and Chemical Biology, Bridgeside Point Building 1, 100 Technology Drive, Pittsburgh, PA 15219

Abstract

The tumor suppressor RNA-binding motif 5 (RBM5) regulates the expression levels and cassette exon-definition (i.e. splicing) of a select set of mRNAs in a tissue-specific manner. Most RBM5-regulated targets were identified in oncological investigations and frequently involve genes which mediate apoptotic cell death. Little is known about the role of RBM5 in the brain. Also, it is unclear if a brain injury may be required to detect RBM5 mediated effects on pro-apoptotic genes due to their low expression levels in the healthy adult CNS at baseline. Conditional/floxed (brain-specific) gene deleter mice were generated to elucidate CNS-specific RBM5 mRNA targets. Male/female mice were subjected to a severe controlled cortical impact (CCI) traumatic brain injury (TBI) in order to increase the background expression of pro-death mRNAs and facilitate testing of the hypothesis that RBM5 inhibition decreases post-injury upregulation of caspases/FAS in the CNS. As expected, a CCI increased caspases/FAS mRNA in the injured cortex. RBM5 KO did not affect their levels or splicing. Surprisingly, KO increased the mRNA levels of novel targets including *casein kinase 2 alpha prime interacting protein* (Csnka2ip/CKT2) – a gene not thought to be expressed in the brain, contrary to findings here. Twenty-two unique splicing events were also detected in KOs including increased block-inclusion of cassette exons 20–22 in *regulating*

Corresponding Author: Travis C. Jackson, Ph.D., University of South Florida, Morsani College of Medicine, USF Health Heart Institute, MDD 0742, 560 Channelside Dr, Tampa FL, 33602, tcjackson@usf.edu.

Author Contributions

TCJ designed the studies. TCJ, PMK, and EKJ wrote the manuscript. TCJ, PMK, EKJ, and KG contributed to data analysis. KJF and VAV performed experiments. KJF, VAV, and KG contributed to editing the manuscript draft.

Conflicts of Interest/Disclosure: Drs. Travis C. Jackson and Patrick M. Kochanek are inventors on a USPTO patent (No. 9,610,266) titled: Small molecule inhibitors of RNA binding motif (RBM) proteins for the treatment of acute cellular injury.

synaptic membrane exocytosis 2 (Rims2). In conclusion, here we used genome-wide transcriptomic analysis on healthy and injured RBM5 KO mouse brain tissue to elucidate the first known gene targets of this enigmatic RBP in this CNS.

Graphical Abstract

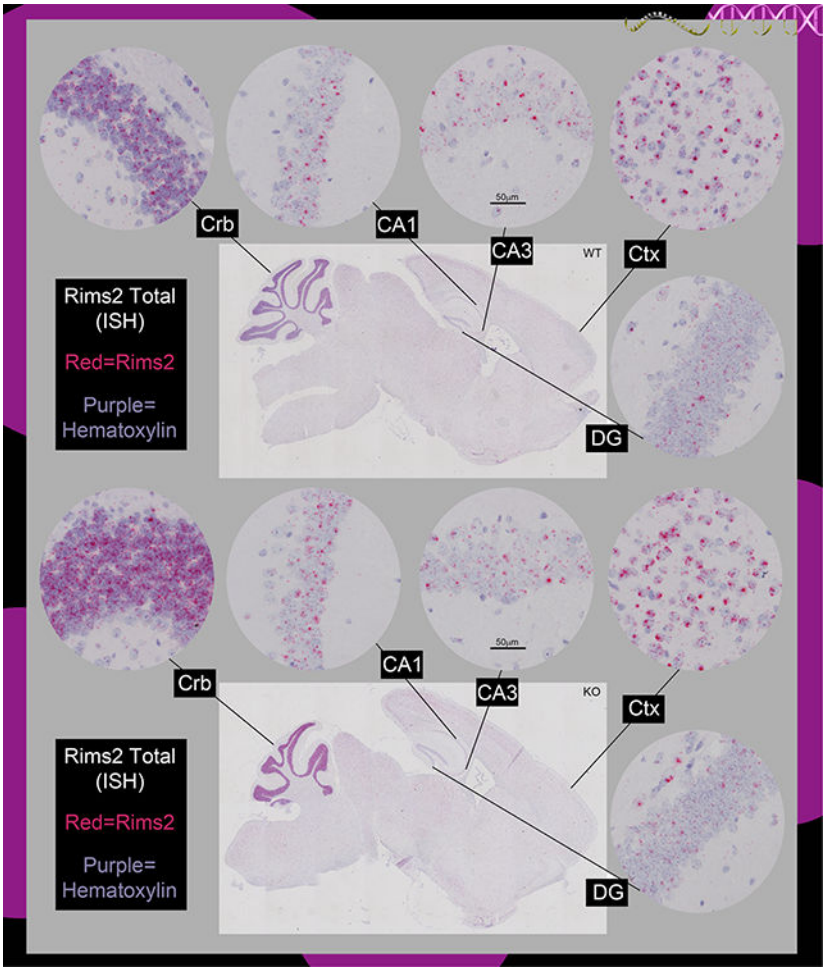

Keywords

RBM5; Rims2; Neurotransmitter; Brain; RNA-Binding Protein; RNA Splicing

Introduction

RNA-binding motif 5 (RBM5) is a member of the RNA recognition motif (RRM) domain-containing family of RNA-binding proteins (RBPs) (Sutherland et al., 2005). Pioneering studies in cancer first demonstrated that it potently activates pro-death pathways in cells (Oh et al., 2006; Oh et al., 2002). The molecular mechanisms that mediate RBM5-dependent tumor suppression involve increased expression of pro-death genes and pre-mRNA splicing events that favor the translation of protein variants with greater toxicity. For instance, RBM5-dependent modulation of caspase-2 splicing in HeLa cells increased the translation

of the long-variant (Casp2L), which is a potent inducer of apoptosis (Fushimi et al., 2008). Similarly, RBM5-dependent modulation of FAS splicing alters the activation of extracellular death receptors in HeLa cells (Bonnal et al., 2008). In addition, endogenous loss of RBM5, or its experimental knockdown, decreases total mRNA levels of caspases, which in turn promotes tumor survival and metastasis of cancers (Mourtada-Maarabouni et al., 2006; Oh et al., 2010). The extent that RBM5 augments the expression of canonical cell death genes (e.g. defined by its targets/effects in cancer) or rather if it modulates non-canonical pathways in normal tissues has not been determined for most organs.

The brain is enriched in RBM5 vs. other tissues yet its role in the CNS is poorly understood (O'Bryan et al., 2013). A total of four articles to date have investigated RBM5 functions in neurobiologically-relevant models (Jackson et al., 2015; Jackson et al., 2018b; Jackson et al., 2017; Zhang et al., 2015). Two studies used primary rat cortical neurons and two studies used immortalized/transformed neuronal cell lines. Three directly confirmed that RBM5 has neurotoxic effects. Collectively, they show that RBM5 promotes neuronal death in models of: (a) mechanical stretch-injury to induce trauma in primary neurons *in vitro* (Jackson et al., 2018b), (b) hydrogen peroxide injury to induce necrosis in rat neuronal pheochromocytoma (PC12) cells (Zhang et al., 2015), and (c) staurosporine injury to induce apoptosis in human differentiated neuronal SHSY5Y cells (Jackson et al., 2015). The gene programs regulated by RBM5 that led to enhanced neuronal vulnerability in these systems were not elucidated. Also, two of the articles included observational studies on the injured rodent CNS and found that endogenous RBM5 protein is increased in the hippocampus after experimental traumatic brain injury (TBI) and in spinal tissue after traumatic spinal cord injury (SCI) (Jackson et al., 2015; Zhang et al., 2015). Thus, RBM5 is increased after CNS damage *in vivo*, and it exacerbates neuronal injury *in vitro*, but the gene pathways mediating the latter effects are unknown.

The remaining (fourth) study investigated RBM5-dependent changes in the global transcriptome in healthy/uninjured primary rat cortical neurons pre-treated with RBM5 targeting RNAi (Jackson et al., 2017). Gene inhibition resulted in increased levels of the small GTPase Rab4a, which in turn increased endocytosis-mediated intracellular uptake of the monomeric serotonin transporter. No alterations in cell death related signaling pathways in RBM5 knockdown neurons were found; however, the omission of a post-injury comparison group may have precluded the detection of canonical cell death genes because their baseline expression is low in healthy neurons and is increased after damage (e.g. caspases). Thus, a paucity of data exists to address if RBM5-regulated pro-death genes and/or splicing events, which have mostly been observed in cancer cells, might manifest in the CNS only after an injury. Also, it has not been tested if RBM5 inhibition *in vivo* alters the expression of pro-death genes in the brain (healthy or injured), or if it alters the regulation of novel targets (e.g. Rab4a) recently identified *in vitro* (Jackson et al., 2017).

Here we addressed these knowledge-gaps by: (1) creating a novel transgenic conditional brain-targeted RBM5 knockout (KO) mouse, (2) subjecting it to an experimental severe TBI to trigger CNS damage and stimulate increased expression of cell death genes, and (3) performing global transcriptomic analysis in WTs vs. KOs to test the hypothesis that RBM5 inhibition robustly decreases the expression of pro-death genes in the brain *in vivo* in an

injury-dependent manner. Novel conditional KOs were created for these studies because homozygous total body KO of RBM5 is postnatally lethal (Jamsai et al., 2017). As expected, TBI increased canonical pro-death RBM5 gene targets in the brain (e.g. caspases and FAS) but contrary to our hypothesis were unaffected by KO. We also found that Rab4a was not increased in the mouse cortex *in vivo* in KOs, which was contrary to expectations based on prior reports in rat cortical neurons *in vitro* (Jackson et al., 2017). Instead, we identified novel RBM5 targets. Genes in the cortex in which total mRNA levels were altered in KOs vs. WTs but in which splicing was unaffected included: casein kinase 2 alpha prime interacting protein (Csnka2ip/CKT2), Gm756, Serpina3n, and glial fibrillary acidic protein (GFAP). Genes in which cassette exon splicing was altered but in which total expression in the cortex was unaffected included: synaptic membrane exocytosis 2 (Rims2), solute carrier family 20 member 1 (Slc20a1), myocyte enhancer factor 2a (Mef2a), and N-myc downstream-regulated gene 2 protein (Ndrg2). In summary, here we report the first known targets of RBM5 in the brain *in vivo*.

Experimental Procedures

Study Design:

The goal of this study was to determine if RBM5 regulates, in the brain, cell death genes that are well-known targets in cancer. We created novel conditional RBM5 KO mice due to the inability to investigate gene expression changes in adult mice using previously established total body RBM5 KOs. Novel transgenics were crossed with Nestin-CRE mice to produce offspring (F2 generation) that were homozygous for RBM5 gene deletion in the brain. Mice were genotyped to confirm both CRE expression and RBM5 allele status. A breeding scheme was employed that ensured all group comparisons in downstream studies (WT, Het, KO sham vs. injury) harbored a single copy of the CRE transgene. A controlled cortical impact (CCI)-TBI was used to increase the expression of pro-death genes in the cortex and to modify the transcriptome in a manner which we hypothesized would optimize the detection of RBM5-mediated effects on caspases/FAS levels should they exist in the brain. A total of seven mice per group were targeted for RNA studies (6 groups in total), which is consistent with numbers used in prior studies to detect gene expression changes by microarray in transgenic mice (McClard et al., 2018; McGill et al., 2018; Medrano and Naya, 2017). A few genes were selected for further validation by quantitative Nanostring and for *in situ* hybridization (ISH) experiments. Acute cardiovascular physiology and weight were characterized in mice that survived to the 48h study endpoint and a total of ten animals per group were targeted. Experiments were designed to limit gender bias by including both male and female subjects in sham and CCI treatment groups for combined gene analysis. Allocation was randomized by: (a) sham vs. injury and (b) the age/sex that mice entered the CCI study based on availability. Acute physiological data and weight were collected and analyzed for animals that survived to the study conclusion (i.e. the 48h tissue collection timepoint). Physiological data was excluded from analysis for one male mouse in the WT-CCI group and for one male mouse in the KO-CCI group because they died prior to the predefined study endpoint (i.e. out of protocol). No sample data was excluded from microarray analysis. Naïve mice were used for ISH studies.

Animals:

All animal work was approved by the Institutional Animal Care and Use Committee of the University of Pittsburgh. Protocols follow recommendations established by the American Medical Veterinary Association Guideline for Euthanasia. Studies were designed to minimize pain and suffering, and to use the minimum number of animals required to achieve significance. Animals were granted ab libitum accesses to food and water. All animals were maintained on 12h light/dark cycle. Animal surveillance of housing facilities and veterinary care are supervised by Division of Laboratory Animal Resources (DLAR) staff. B6.Cg-Tg(Nes-cre)1Kln/J mice were purchased from JAX (The Jackson Laboratory; Stock No: 003771). Nestin-CRE mice were maintained in the hemizygous (single copy) state for LoxP recombination studies and for colony maintenance. Novel transgenic conditional RBM5 KOs were created by goGermline technology (Ozgene; Bentley DC, WA, Australia). In brief, C57BL/6 ES cells were electroporated with a targeting vector which included LoxP-flanked exon 3 of the RBM5 gene and a FRT-flanked neomycin (Neo) cassette. Transgene insertion was confirmed by antibiotic resistance and southern blotting. ES mutant clones were injected into donor blastocysts and implanted into psudopregnant recipient female mice. Chimeric mice were identified by coat color and bred to germline transmission. Heterozygous C57BL/6 $Rbm5^{tm1Ozg}$ mice were crossed with FLP deleters to remove the Neo cassette. Male founders were crossed with C57BL/6 female wild-type (WT) mice purchased from JAX laboratories. Heterozygous $Rbm5^{tm1Ozg}$ mice were crossed to generate homozygous $Rbm5^{tm1Ozg}$ mice. F1 colonies were generated by crossing homozygous $Rbm5^{tm1Ozg}$ mice with hemizygous B6.Cg-Tg(Nes-cre)1Kln/J mice. F1 heterozygous $Rbm5^{tm1Ozg}$ mice without CRE were breed with F1 heterozygous $Rbm5^{tm1Ozg}$ mice with CRE, to generate F2 littermates for experiments.

Genotyping:

Tail snips were collected from pre-weaning (16–18d) pups and DNA was isolated for genotyping using Promega Wizard SV Genomic Purification System (Promega; Madison, WI, USA), per the manufacturer's instructions. PCR reactions were run on a Biorad T100 Thermalcycler (BioRad; Hercules, CA, USA). Samples were loaded onto 3% agarose gels with Syber Safe Stain (ThermoFisher Scientific; Waltham, MA, USA). The following primer pair was used to screen pups for the absence or presence of the Cre transgene: GCGGTCTGGCAGTAAAAACTATC (forward) and GTGAAACAGCATTGCTGTCACTT (reverse). The temperature protocol steps were: 94°C/3min, 94°C/30sec, 51.7°C/1min, 72°C/1min repeated for 35 cycles, and 72°C/2min. The presence of the CRE transgene resulted in a ~100bp PCR product. The following primer pair was used to confirm Neo elimination after breeding with FLP deleter mice: ATACGCTTGATCCGGCTACCTG (forward) and TGCAGCCTATCTTCTATAAGGG (reverse). The following primer pair was used to genotype WT, conditional Het, and conditional KO $Rbm5^{tm1Ozg}$ mice, prior to crossing with CRE mice: GCGGGACTCAGATTACAAAAGATC (forward) and TGCAGCCTATCTTCTATAAGGG (reverse). The temperature protocol steps were: 98°C/3min, 98°C/10sec, 62°C/30sec, 72°C/2min repeated for 29 cycles, and 72°C/10min. Samples were loaded onto 0.8% agarose gels with Syber Safe Stain. WT cDNA produced a single ~317pb product, whereas homozygous conditional $Rbm5^{tm1Ozg}$ KO cDNA produced a single ~420bp PCR product.

Controlled Cortical Impact (CCI):

Male/female Nestin-CRE expressing RBM5 WTs, Hets, and KOs were used at 12–15 wks of age. On the day of surgery mice were anesthetized with 4% isoflurane (via nosecone) and decreased to 2% for maintenance anesthesia, in Nitrous Oxide (N_2O)/%O_2 (2:1). MAP and heart rate HR were continuously monitored via a femoral arterial catheter that was surgically inserted. Shams received surgical preparations but did not receive a craniotomy. Mice randomized to TBI were given a CCI as described by our group (Jackson et al., 2018a; Jackson et al., 2015). Our standard insult level (6m/s, 1.2mm depth) produces a moderate-severe TBI, resulting in a substantial ipsilateral cortical lesion post-injury (Jackson et al., 2018a). Tissues for total RNA were harvested 48h post-injury. A total of 42 cortices were harvested for total RNA (n=7/group) as follows: WT-Sham (n=3 male and n=4 female), WT-CCI (n=3 male and n=4 female), Het-Sham (n=3 male and n=4 female), Het-CCI (n=3 male and n=4 female), KO-Sham (n=4 male and n=3 female), KO-CCI (n=3 male and n=4 female). A total of 28 arrays were purchased to analyze the transcriptome in sham/injured WTs vs. KOs. In addition, WT, Het, and KO samples were analyzed in confirmatory Nanostring studies on selected genes (n=7/group).

Blood Chemistry and Weight:

A total of n=10/group were used for acute physiological analysis. Blood (~60μL) was sampled from the arterial catheter at baseline (2% isoflurane in N_2O/%O_2, 2:1), 5 min prior to a CCI (2% isoflurane in room air), 5 min post-CCI (2% isoflurane in room air), and 60 min post-CCI (2% isoflurane in room air). Blood was immediately analyzed via an ABL90 Radiometer Blood Gas Machine (Radiometer Medical ApS; Copenhagen, Denmark), as reported previously by our group in the CCI mouse model (Jackson et al., 2018a). Body weight was recorded prior to injury.

Western blot:

In brief, sham male (n=2 WT and n=2 KO) and sham female (n=2 WT and n=2 KO) hippocampal extracts were prepared in radioimmunoprecipitation assay (RIPA) buffer supplemented with EDTA, protease inhibitors, and phosphatase inhibitors (ThermoFisher Scientific). Protein concentration analysis was done by the BCA method (ThermoFisher Scientific). ~20μg/well total hippocampal extracts were loaded onto a 4–15% TGX™ pre-cast SDS-PAGE gel (BioRad). Linearized proteins were transferred to a PVDF membrane. Total protein analysis was done using reversible Swift Membrane Stain™ (ThermoFisher Scientific) and images collected via a 600dpi scanner to confirm equal protein loading/transfer. The membrane was blocked and then incubated overnight at 4°C with 1:1000 anti-RBM5 antibody (Proteintech; Chicago, IL, USA - Cat# 19930-1-AP, Lot#49598) diluted in tris-buffered saline tween-20 (TBST) and 7.5% milk. The following day, the membrane was washed, incubated 2h with a secondary antibody, washed again, incubated in ECL-2 detection substrate (Thermo Fisher Scientific), and imaged on film in a dark room. Images were compiled in Photoshop (Adobe; San Jose, CA, USA).

RNA Isolation:

Cortical brain tissues were homogenized in Trizol® in a BeadMill® (ThermoFisher Scientific) set to shake for 60 sec at 3 m/sec with 2.8 mM ceramic beads. A 1:5 volume of chloroform to Trizol was added and vigorously shaken. The mixture was incubated 15 mins at room temperature. Samples were centrifugated 15 mins at 12,000g to induce phase separation. The aqueous phase was isolated and placed in a new microcentrifuge tube. RNA was precipitated by addition of a 1:1 volume of isopropanol to sample (equal to the aqueous extraction volume). The RNA pellet was washed with 75% ethanol, air dried, and resuspended in nuclease-free water. The OD260, 260/280, and 260/230 ratio were measured by Nanodrop (ThermoFisher Scientific) to determine RNA concentration and purity. The integrity of RNA was confirmed by Tape Station® 4200 (Agilent; Santa Clara, CA, USA). The eRIN was >8.4 for all samples.

Microarray Analysis:

Complementary DNA (cDNA) was prepared using the WT Plus reagent kit (ThermoFisher Scientific) and used according to manufacturer instructions. Reverse transcription was done with 100ng total RNA and dNTP-T7 random primers. Second strand synthesis and *in vitro* transcription was done to amplify cRNA. A second reverse transcription reaction produced cDNA which was fragmented and end-labeled with biotin for hybridization onto Clariom D (MTA-1_0) arrays (5μg ds cDNA per array). After overnight (~16h) hybridization at 45°C, with rotational mixing at 60 rpm, arrays were processed on a GeneChip® 450 Fluidics Station (ThermoFisher Scientific) using manufacturer specified protocols. To remove unbound sample, arrays were washed with non-stringent *wash buffer A*. The GeneChips® were stained 10 mins in *Stain cocktail 1*. Excess stain was removed with *wash buffer A*. Signal amplification was achieved by 10 mins incubation with *Stain Cocktail 2* followed by 10 min incubation with *Stain Cocktail 1*. The chips were washed with high stringency *Buffer B* and prior to removal from the fluidics station, loaded with *Array Holding Buffer*, then scanned using the GeneArray® 3000 scanner (ThermoFisher Scientific). Data quality-control and statistics were performed with Transcriptome Analysis Console (TAC) 4.0. Affymetrix/ThermoFisher Expression Console (EC) software was used for RMA normalization prior to DEG/splicing analysis. Microarray data (chp. and CEL. Files) were uploaded to the NCBI Gene Expression Omnibus database. All individual arrays passed labeling control-threshold QC, hybridization control-threshold QC, and Pos. vs. Neg. AUC Threshold QC.

Quantitative mRNA Analysis:

Custom NanoString nCounter gene expression codesets were developed. Brain tissue RNA was processed on the NanoString nCounter Analysis System according to the manufacturer's protocol (NanoString Technologies; Seattle, WA, USA). Briefly, 100ng of RNA was hybridized to the reporter probes and capture probes in a thermal cycler for 16 hours at 65°C. Washing and cartridge immobilization was performed on the nCounter PrepStation (NanoString Technologies) and the cartridge was scanned at 555 fields of view on the nCounter Digital Analyzer (NanoString Technologies). The resulting RCC files

containing raw target counts were imported into the NanoString nSolver Analysis Software v4.0 (NanoString Technologies) for downstream normalization and analysis.

High-Fidelity Single-Molecule ISH:

Naïve adult male WT and KO mice were used for RNA analysis on brain slices. FFPE brain tissue sections were prepared as described by our group and with minor modifications per manufacturer's recommendations for ISH (Jackson et al., 2018a). For each ISH experiment, WT vs. KO brains were placed on the same glass slide to ensure equivalent manipulations across genotypes. RNA in situ hybridization experiments were performed using RNAscope® (Advanced Cell Diagnostics; Newark, CA, USA) as described by others (Wang et al., 2012). This technique enhances the rigor of ISH by robustly increasing the signal-to-noise ratio to detect individual mRNA molecules with high specificity by utilizing contiguous binding pairs of short target probes, which in the correct order, permits a subsequent preamplifier probe to bind and results in a signal (amplifier) (Wang et al., 2012). Paired double-Z oligonucleotide probes were designed against target RNA using custom software (Advanced Cell Diagnostics). The following probes were used: Mm-Csnka2ip, cat no. 824601, ENSMUST00000089279.4, 20zz pair, nt 134–1271; Mm-Rims2-O1, cat no. 824591, ENSMUST00000042917.9, 13zz pair, nt 2055–2842; BA-Mm-Rims2-E22E23, cat no. 824581, NM_001256382.1, 1zz pair, nt 4072–4113; BA-Mm-Rims2-E19E20, cat no. 824571, NM_001256382.1, 1zz pair, nt 3554–3598. The RNAscope® and BaseScope™ Reagent Kit (Advanced Cell Diagnostics) was used according to the manufacturer's instructions. High RNA integrity was confirmed for each sample with a probe specific to the housekeeping gene cyclophilin B (PPIB). Negative control background staining was evaluated using a probe specific to the bacillus subtilis dihydrodipicolinate reductase gene (dapB). Brain slices were counterstained with Hematoxylin. Total Csnka2ip and Rims2 mRNAs were detected with the 2.5 HD Red Assay Kit (Advanced Cell Diagnostics). Rims2 splice variant probes were detected with the BaseScope RED assay kit (Advanced Cell Diagnostics). The technician performing ISH staining was blind to genotype. The technician performing Image-J analysis was blind to genotype and to the target under investigation. Images were scanned at 4X and 20X. Randomly selected fields, within comparative brain sub-regions, were collected for enhanced viewing of 20X staining in ISH figures. Staining intensity was measured in Image-J. In brief, images were first deconvoluted to blue, green, and red signals. Pixels for the red probe-staining signal (color 2) were measured for each target. Thresholding was adjusted for each target and then consistently applied across all brain regions and genotype for a given probe. Three equivalent size boxes were drawn at random in each 20X image (i.e. three ROIs). Box sizes were identical across all images. The percent area containing signal within each box was calculated (unitless value) and the results averaged for each image. The fold-change was calculated by dividing the mean pixel content computed for each brain region/target in KOs by the mean pixel content in WTs. A decrease or increase in signal staining was defined as a fold-change < -2 or > 2, respectively.

Statistical Analysis:

Microarray: The filter criteria for significance for *differentially expressed genes (DEGs)* was: Fold-change > 2 or < -2 *AND* FDR-corrected p-value <0.05. The filter criteria for significance for *splicing events* was: (a) gene target expressed in both conditions, (b)

exon/PSR within gene target expressed in at least one condition, (c) splicing Index > 2 or < −2, (d) FDR-corrected exon p-value <0.05, and (e) exon event score >0.2. A probe set (gene/exon) was considered expressed if ≥ 50% samples have detected above background (DABG) levels below threshold (0.05). Data were analyzed by ANOVA and FDR adjusted p-values were based on Benjamini-Hochberg Step-Up FDR-controlling Procedure. Exon event scores were calculated based on EventPointer (Romero et al., 2016). *Nanostring:* Significance was determined by a two-tailed t-test of the log-transformed normalized data within the nSolver Software Package. All samples passed QC parameters. Expression data was normalized to the geometric mean of: (a) spiked positive controls to adjust for technical variations across lanes and cartridges, and (b) to the geometric mean of five housekeeping genes (GAPDH, GUSB, LDHA, Olfr776, PGK1) for codeset content normalization. The reference gene list was collated based on a literature review of housekeeping targets that yielded best results for quantitative gene expression analysis studies and based on empirical confirmation of stably expressed genes in our microarray studies (Boda et al., 2009; Kang et al., 2018). Normalized counts of gene targets (n=7/group) were imputed into Prism and represented as box plots which show the minimum value, maximum value, interquartile range (IQR), and median (GraphPad Software Inc; La Jolla, CA, USA). *Acute Physiology:* MAP, HR, and blood chemistry data were analyzed by 3-Way-ANOVA. Body weight was analyzed by 2-Way ANOVA and using a Tukey's Multiple Comparison post-hoc test. Data were significant at two tailed $p<0.05$.

Accession Codes:

The accession number for raw microarray data submitted to NCBI GEO is **GSE128543**.

Results

Validation of Novel Conditional RBM5 KO Mice.

A conditional gene targeting strategy was designed (Fig. 1A) and KO was confirmed by PCR genotyping (Fig. 1B) and by Western blot analysis in mouse hippocampal tissue extracts (Fig. 1C). RBM5 migrated at ~120 kDa on SDS-PAGE, consistent with our prior reports in primary rat cortical neurons (Jackson et al., 2018b; Jackson et al., 2017). Homozygous brain-specific RBM5 KOs were viable, well-appearing at birth, and showed no overt signs of health and/or behavioral abnormalities in adulthood. Mendelian ratios were calculated from F2 litters bred between August 2017 to January 2019 for mice that expressed a single copy of the CRE transgene (Fig. 1D). WTs (~28%) and Hets (~50%) followed the expected ratios. In contrast, the number of brain-specific KOs was lower than expected (~15%). Decreased KO numbers was not due to increased postnatal mortality, as was previously reported to occur in total body RBM5 KOs (Jamsai et al., 2017). Furthermore, the phenomenon was independent of sex - 13 male KOs vs. 10 females KOs survived into adulthood. In the course of studies two adult KOs died of unknown causes (1 Male and 1 Female; both >2mo of age), and a single male KO was euthanized postnatally because it was a runt. The mechanism(s) mediating a decrease in the number of KOs remains to be elucidated.

Next, we measured mean arterial blood pressure (MAP), heart rate (HR) and hematological parameters to characterize baseline cardiovascular health in RBM5 KO shams and in injured mice. We focused on characterizing global cardiovascular indices here because they profoundly affect brain tissue survival and thus gene expression changes in the acute period after a TBI (Kroppenstedt et al., 1999). There were no differences in MAP (Fig. 2A) or HR (Fig. 2B) in WTs vs. KOs at baseline or after a CCI. KOs weighed significantly less vs. WTs (~3g). This effect was independent of sex and not seen in heterozygotes (Fig. 2C). There were no genotype differences in arterial pCO_2, or pO_2, or SaO_2, hematocrit, hemoglobin, HCO_3, potassium, or lactate (Fig. 2D). In contrast, blood sodium, chloride, glucose and osmolality were significantly (albeit modestly) increased in KOs vs. WTs (Fig. 2D). In addition, KOs had a slight decrease in blood pH. The differences were minor and all blood chemistry values in WTs and KOs were within the normal range for anesthetized mice. Heterozygotes also had significant (albeit minor) differences in blood sodium, chloride, glucose and osmolality vs. WTs but were detected as an interaction term and were within the normal range (Table S1). In summary, global measures of cardiovascular function and blood chemistry were comparable between WT vs. KOs before and immediately after a brain injury.

RBM5 KO does not Decrease TBI-Induced Upregulation of Cell Death Genes in the Injured Cortex.

In WTs, CCI injury altered the expression of 154 coding-gene mRNAs (145 increased and 9 decreased) (Fig. 3A). Moreover, 203 multiple-complex genes were significantly altered by injury (194 increased and 9 decreased). Gene ontology (GO) analysis in PANTHER14.1 on the combined coding/multi-complex genes in WT mice mapped 166 genes across 57 distinct areas (Ashburner et al., 2000; Carbon et al., 2019; Mi et al., 2019) (Fig. 3B and Fig. S1). Injury-related pathways of note are highlighted in Fig. 3B. Microarray analysis confirmed a significant increase in caspase-8 expression levels in WT mice (CCI vs. sham; Table S2). In addition, caspase-4 and FAS levels trended to increase after a CCI (Table S2). Nanostring quantification confirmed a significant increase in the mRNA levels of caspase-4 (Fig. 3D), caspase-8 (Fig. 3G), and FAS (Fig. 3H) in the cortex in injured WTs vs. shams. Contrary to our hypothesis, RBM5 gene KO did not decrease the levels of caspases/FAS after a CCI (Fig. 4A–F and Table S2). In summary, global transcriptomic analysis suggests that RBM5 does not regulate mRNA expression of canonical cell death gene targets in the acute period after a TBI.

Novel Gene Targets of RBM5 in the Brain: Csnka2ip is Expressed in the CNS & is Regulated by RBM5.

A total of four coding or multiple-complex genes were differentially expressed in WTs vs. KOs as determined by global transcriptomic analysis and included: casein kinase 2 alpha prime interacting protein (Csnka2ip/CKT2), Gm756, Serpina3n, and GFAP (Fig. 5A). We focused downstream confirmatory studies on Csnka2ip because it was the most significant coding gene identified (FDR p-value 10^{-7}) and because prior studies reported it was not expressed in the brain. The mouse gene ensemble database predicts two Cnska2ip transcripts (201 and 202). Nanostring probes were designed to measure the levels of each transcript separately. Cnska2ip-201 was significantly increased in sham KOs vs. sham WTs (Fig. 5B)

and in CCI-injured KOs vs. CCI-injured WTs (Fig. 5C), which was consistent with microarray findings. In contrast, Cnska2ip-202 was unaffected by KO and was not the dominant transcript expressed in the brain (Fig. 5B and 5C). Prior studies in rat cortical neurons found that RBM5 inhibition robustly increased mRNA levels of the small GTPase Rab4a (Jackson et al., 2017). Surprisingly, Rab4a was not among the differentially expressed genes detected in microarray studies on cortical tissue here. We confirmed this finding with Nanostring. The mouse gene ensemble database predicts three Rab4a transcripts and two are protein coding (201 and 202). Rab4a-202 was the dominant coding transcript in the brain. Consistent with the results of microarray, Nanostring analysis did not show increased levels of either transcript in the KO cortex (Fig. 5D and Fig. 5E). Finally, to further confirm and characterize Cnska2ip expression in the brain, ISH analysis using high-sensitivity RNAscope® technology was done to visualize the distribution of Cnska2ip-201 transcripts in sagittal brain sections. Csnka2ip staining was seen in the cerebellum, hippocampus (CA1, CA3, and DG), and in the cortex in both WTs (Fig. 6A–E) and KOs (Fig. 6F–J). Semi-quantitative Image-J analysis did not reveal a 2-fold increase in Cnska2ip staining in the KO vs. WT cortex as was seen with quantitative microarray and Nanostring (Fig. 11). In summary, brain-targeted RBM5 KO increased the levels of several novel gene targets including Cnska2ip in the cortex but did not alter Rab4a levels.

Novel Splicing Targets of RBM5 in the Brain

We first analyzed global splicing changes in WT mice (CCI vs. sham) to better characterize splicing events manifesting after injury in our experimental mouse model of TBI. 248 genes (out of 65,770) representing 0.37% of the total analyzable genome using current arrays passed filter criteria in support of alternative splicing (Fig. S2). A total of 564 events were detected among the 248 genes (Fig. S2). Most events were cassette exons (341/564). GO analysis in PANTHER14.1 mapped 174 of the 248 genes. (Fig. S2B and S2C). The effect of alternative splicing on altered protein function(s) are unknown for most mammalian genes. Nevertheless, Fig. S2B highlights a few notable splicing events which were robustly detected in our analysis and warrant future study as they may be important in understanding mechanisms of secondary brain injury after a TBI (i.e. beyond the primary goal of this study). Key targets included changes in the levels of cassette exons for caspase-8, matrix metallopeptidase 12 (MMP-12), serpina3g/Spi2A, TNF receptor superfamily member 1A (TNFR1), GFAP, tissue inhibitor of metalloproteinase 1 (TIMP-1).

Next we compared splicing changes in KOs vs. WTs in the cortex. A total of 22 events passed filter criteria and were affected by genotype in our primary analysis (Fig. 7A). The splicing events were largely independent of injury (i.e. the magnitude of the difference was similar in KO shams or KO CCI vs. WTs). Thus, we collapsed datasets by genotype for a secondary analysis (n=14 KOs and n=14 WTs) to screen for additional potential splicing events which may have evaded detection in the primary analysis. Three additional potential splicing events were found (Fig. 7A; Blue Columns). Fig. 7B shows an example of the microarray probe-level values for PSRs/junctions in the Rims2 gene. We were particularly interested in Rims2 splicing changes because RBM5 KO resulted in increased levels of three different cassette exons in that gene.

Next we performed confirmatory NanoString studies on genes which harbored alternately spliced cassette exons found in the primary analysis and also verified the intron-retention event in myeloid leukemia factor (Mlf2) because it had a notably robust degree of significance (i.e. FDR p-value of 10^{-9}). Custom probes were designed to anneal at specified junctions (Table S3): Rims2 (exons 19–23 , exons 21–22, and at a loci outside of known splice sites), Mef2a (exons 5–6), Ndrg2 (exons 2–3), Slc201a (exons 5–6), Lrrc49 (exons 3–5 and exons 9–10) and, Mlf2 (intron 8-exon 8 and intron 8-exon 9). A custom probe to measure the cassette exon event in Phkb could not be designed and was removed from further confirmatory analysis. Rims2 transcripts containing a contiguous exon 19–23 were decreased in KOs vs. WTs (Fig. 7C; Probe 1, top blue panel). Rims2 transcripts containing a contiguous exon 21–22 were increased in KOs vs. WTs (Fig. 7C; Probe 2, bottom blue panel). Rims2 transcripts targeting regions outside of known splice sites (i.e. measures total mRNA levels) were not statistically different in KOs vs. WTs (Fig. 7C; Probe 3, bottom pink panel). A protein alignment analysis of exons 20–22 in the mouse Rims2 transcript- 201 vs. the human Rims2 transcript-204 in LALIGN indicated 93.6% identity indicating conservation of these splice sites in humans (Fig. S3). Heterozygous mice also had significantly increased levels of Rims2 transcripts containing contiguous exons 21–22 vs. WTs (Fig. S4).

Mef2a Nanostring findings supported microarray results; a probe which overlapped with the spliced exon 5 was significantly decreased in KOs vs. WTs (Fig. S5B). Ndrg2 Nanostring findings also supported microarray results; a probe which measured the levels of transcripts that exclude (skip) exon 3 was decreased in KOs vs. WTs (i.e. suggesting that exon 3 is increased in KOs; Fig. S5C). Slc20a Nanostring findings supported microarray results – a probe which overlapped with the spliced exon 6 was significantly decreased in KOs vs. WTs (Fig. S5D). Lrrc49 Nanostring findings were incongruent with microarray findings and did not confirm altered splicing of exon 4 or exon 10 (Fig. S5F and S5G, respectively). Mlf2 Nanostring findings supported microarray results; a probe which measured the boundary of intron 8 and exon 9 was robustly decreased in KOs vs. WTs (Fig. S5H). Germane to Slc201a, heterozygous mice also had decreased levels of exon 6 (Fig. S4).

Rims2 changes were among the most robust cassette-exon splicing events detected in our transcriptomic analysis in KOs and was present in heterozygotes. Thus, we focused further ISH staining characterization efforts on Rims2 splicing changes. First, total Rims2 mRNA staining was visualized and found to be widespread in the cerebellum, hippocampus (CA1, CA3, and DG), and in the cortex in both WTs (Fig. 8A–E) and KOs (Fig. 8F–J). Semi-quantitative Image-J analysis revealed a ~4-fold increase in total Rims2 staining in KOs in the cerebellum and was associated with altered morphology of the cerebellar folia (Fig. 8A vs. 8F and Fig. 11). RNAscope® controls confirmed the specificity/sensitivity of the assay. No staining was seen in the negative control (bacterial gene dapB; Fig. S6). The positive control stain PPIB was equivalent and widespread in the cerebellum, hippocampus (CA1, CA3, and DG), and in the cortex in WTs and KOs (Fig. S7). Notably, PPIB staining was similar in the WT vs. KO cerebellum (Fig. S7A vs. S7F and Fig. 11).

Next, Rims2 transcripts harboring specific splicing events were visualized using BaseScope™ technology. To further compliment Nanostring and microarray investigations,

custom ISH probes were designed to selectively target the proximal and distal regions of the triexon block splice sites which were not analyzed in the Nanostring study (e.g. Probe 1: Rims2 exon junction 19–20, and Probe 2: Rims2 exon junction 22–23). Rims2 E19-E20 staining (Fig. 9 and Fig. 11) and Rims2 E22–23 staining (Fig. 10 and Fig. 11) were increased (> 2-Fold) in KOs vs. WTs. Notably, semi-quantitative Image-J analysis revealed that the largest increase was in all fields of the hippocampus. (e.g. Fig. 9B vs. 9G, 9C vs. 9H, 9E vs. 9J and Fig. 11). BaseScope™ controls confirmed the specificity/sensitivity of the assay. No staining was seen with the negative dapB (Fig. S8). PPIB staining (positive control) was widespread in WT and KOs but did not differ by genotype (Fig. S9 and Fig. 11). In summary, brain-targeted RBM5 KO altered splicing of several novel gene targets including Rims2.

Discussion

RBM5 is increased in the mouse brain after an experimental TBI (Jackson et al., 2015). We speculated that its upregulation after trauma might promote the expression of pro-death genes in the CNS based on its well-known tumor suppressor functions in cancer. However, a single report on RBM5 gene targets in neurons did not find evidence that it regulates cell death pathways in uninjured-healthy cells (Jackson et al., 2017). Thus, we hypothesized that RBM5 may promote the expression and/or alter the splicing of cell death genes only after injury. Here we used the CCI-TBI model, a well-established tool to study a broad spectrum of pro-death genes/pathways in the brain, to test *in vivo* our primary hypothesis that RBM5 inhibition decreases pro-death gene expression in the injured cortex (Clark et al., 2000; Franz et al., 2002; Newcomb et al., 1999). Moreover, we created novel conditional KOs to minimize confounding cardiovascular effects or other peripheral changes induced by total body gene manipulations, and also to avoid postnatal death in RBM5 null pups which was seen in other strains (Jackson et al., 2018a; Jamsai et al., 2017).

As expected, CCI increased the expression of pro-death genes including caspase-8, caspase-4, and FAS. Brain-specific RBM5 gene deletion did not affect their expression level or RNA-splicing. Additional studies are needed to evaluate our primary hypothesis in different models of CNS injury and to measure potential changes in the transcriptome at later stages postinjury. In addition to cell death genes, studies in cortical neurons reported that Rab4a is a novel target regulated by RBM5 *in vitro* but we did not detect differences in the cortical levels of this gene in WTs vs. KOs *in vivo*; the reason for that discrepancy is unclear but may relate to differences in the experimental design between studies (e.g. species investigated, developmental stage of neurons, the influence of culture media on background gene expression, or the composition of the transcriptome in homogenous cortical neurons vs. heterogenous cortical brain tissue). Despite the lack of evidence to support the concept that RBM5 increases the expression of canonical pro-death genes in the injured brain, others have shown that it promotes neurotoxicity in diverse models of neuronal injury *in vitro* (Jackson et al., 2015; Jackson et al., 2018b; Zhang et al., 2015). Thus, it is possible that RBM5 enhances neuronal vulnerability via novel mechanisms which differ from those activated in cancer. That concept merits further investigation.

Csnka2ip was a surprising target identified in our screen. RBM5 KOs (shams and CCI-injured) had increased mRNA levels of Csnka2ip in the cortex vs. WTs. The seminal study on Csnka2ip reported that mRNA levels were undetectable in the mouse brain and found that it was exclusively expressed in the testes (Bai et al., 2009). The authors performed reverse-transcription PCR followed by gel electrophoresis to visualize PCR products. We do not know why our findings deviated from prior work. Both false-negative and false-positive findings in traditional RT-PCR studies have been widely discussed (Lion, 2001). Nevertheless, we used three markedly different and ultra-sensitive techniques (contemporary microarrays, Nanostring, and high-fidelity ISH) to confirm Csnka2ip expression in the mouse brain in WTs and in KOs.

The function of Csnka2ip in neurons is unknown. To our knowledge only two articles have reported on facets of its regulation (Bai et al., 2009; Liao et al., 2016). Mechanistically, it binds to the catalytic subunit of casein kinase 2 alpha prime (CK2α') and is phosphorylated by the latter (Bai et al., 2009). Phosphorylated Csnka2ip is detectable in testicular lysates from WT mice but not in CK2α' KOs (Bai et al., 2009). Germane to the brain, CK2α' is widely distributed across the CNS and CK2 proteins phosphorylate over 300 substrates (Castello et al., 2017; Meggio and Pinna, 2003). Thus, Csnka2ip may play an important role in the regulation of signaling cascades in the brain. According to the mouse gene ensemble database there are two protein coding Csnka2ip transcripts. Transcript-201 encodes a small 276 amino acid (~30kDa) protein, and transcript-202 encodes a large 720 amino acid (~80kDa) protein. The small protein in specific was found to bind CK2α' in mouse testes and modulate signal transduction (Bai et al., 2009). RBM5 KO increased the small (201) but not the large (202) transcript. Csnka2ip ZZ probe pairs in ISH studies were designed against regions within the mouse 201 transcript. Image-J analysis of ISH data did not indicate a > 2-fold increase of Csnka2ip levels in the KO vs. WT cortex as was seen with microarray and Nanostring. The lower sensitivity and semi-quantitative nature of staining analysis may explain the discrepancy. No commercial anti-Csnka2ip antibodies are currently available. Thus, future studies are needed to confirm the presence of brain Csnka2ip at the protein level pending the development and validation of the necessary reagents.

There is limited data on global gene-splicing changes in models of TBI (Meng et al., 2017). Therefore, we think it worthwhile to highlight some notable splicing alterations detected in our analysis in WT mice before discussing the effects of KO. *Caspase-8:* Exon 3 skipping in caspase-8 results in an anti-apoptotic short variant (caspase-8s) (Kisenge et al., 2003). In our analysis exon 2 and 3 in caspase-8 decreased 2.65-fold and 2.72-fold (i.e. splicing index/SI) after a CCI. *MMP-12:* MMP-12 promotes blood brain barrier damage after focal ischemic stroke (Chelluboina et al., 2015). We found that exon 4 in MMP-12 increased 4.48-fold (SI) after a CCI. *Serpina3g:* Cathepsin B is a cysteine protease which mediates cell death and contributes to TBI-induced tissue injury (de Castro et al., 2016; Hook et al., 2015). Relatedly, Serpina3g/Spi2A is a potent cathepsin B inhibitor (Liu et al., 2003). We found that Exon 4 in the Serpina3g transcript increased 43.32-fold (SI) after a CCI. *TNFR1:* TNFR1 redistributes to lipid rafts after TBI and mediates neuronal death (Lotocki et al., 2004). In our analysis exon 3 in TNFR1 increased 3.87-fold after a CCI. *GFAP:* GFAP is a clinical biomarker in TBI prognostication (Bazarian et al., 2018). Exon 1 in GFAP decreased 21.9-fold after CCI in our study. *TIMP1:* Overexpression of tissue inhibitor of

metalloproteinase 1 (TIMP-1) decreases brain lesion volume after a CCI in mice (Tejima et al., 2009). Exon 3, exon 4, and exon 5 in TIMP-1 increased 7.01-fold, 5.57-fold, 3.52-fold, respectively, after a CCI. None of these injury-dependent splicing events were affected by RBM5 KO.

A total of 22 differentially expressed splicing events were detected in our primary analysis of cortical brain tissue in KOs vs. WTs. The limited number of splicing events that differed in KOs may be due to functional redundancies in other closely related RBM paralogues (e.g. RBM6/RBM10). Consistent with that possibility, RBM5 knockdown in HeLa cells failed to alter FAS splicing (as seen here in the brain) unless RBM6 and RBM10 were simultaneously coinhibited (Bonnal et al., 2008). Another possibility is that RBM5 regulates a limited set of gene targets. Indeed, Bechara and colleagues individually knocked down RBM5, RBM6, or RBM10 in breast cancer cells and found a total of 30, 252, or 302 alternative splicing events, respectively (Bechara et al., 2013). Thus, the total number of splicing events induced by selective RBM5 inhibition in the Bechara study was similar to our observations here. The authors found little overlap in the genes affected by inhibition of each RBM (Bechara et al., 2013).

Microarray discoveries on KO-dependent changes in Slc20a1, Mef2a, Ndrg2, and Rims2 splicing were validated by Nanostring. Rims2 captured our interest the most, in part, because it is involved in neurotransmission. RBM5 KOs had increased inclusion of exons 20, 21, and 22 in the Rims2 transcript. This finding was confirmed by three different approaches and four different probes targeting the: (a) E19-E22 junction, (b) E21-E22 junction, (c) E19-E20 junction, and (d) E22-E23 junction (Fig. S10). In addition, these splicing events were seen in multiple brain regions including in the cortex and in the hippocampus. The simultaneous block-splicing of exons 20–22 was predicted in an analysis of the mouse Celera genome database in 2002 and termed "*Splice Site C*" (Wang and Sudhof, 2003). The three exons referenced in that report were identified as 23, 24, and 25 and later revised (e.g. currently exons 20–22 in transcript Rims2–201). The authors also predicted that the block-exclusion of exons 20–22 had functional importance because it kept the transcript in-frame (yielded a protein product), whereas individual splicing of 20, 21, or 22 alone did not (Wang and Sudhof, 2003). To the best of our knowledge RBM5 is the first known regulator of *Splice Site C*. Future studies are needed to elucidate the precise molecular mechanisms mediating altered Rims2 splicing and if RBM5 exerts a direct vs. indirect effect on cassette exon definition. Notably, *Splice Site C* is predicted to be present in the human Rims2 gene (Wang and Sudhof, 2003). Also, protein alignment analysis of exons 20–22 in the mouse Rims2 transcript-201 vs. the human Rims2 transcript-204 indicated 93.6% shared identity.

The effect that *Splice Site C* has on the function of the Rims2 protein is unknown. Rims2 plays a critical role in neurotransmitter dynamics and tethers Ca^{2+} channels to the active zones of synapses. Rapid synchronous neurotransmitter release is severely impaired in double Rims1/2 KOs (Kaeser et al., 2011). Also, selective Rims2 KOs have decreased spontaneous and evoked neurotransmitter release in neurons but no change in Ca^{2+} responsiveness or release synchronization (Kaeser et al., 2012). The spliced region is near the c-terminal C_2B domain, which is essential to bind the ubiquitous β4 subunit of voltage-dependent calcium channels (Kiyonaka et al., 2007; Wang and Sudhof, 2003).

The clinical significance of altered Rims2 signaling in the brain is unclear but is emerging as a potential target in neurological conditions. Mice exposed to open-field blast-TBI showed changes in Rims2 phosphorylation in the brain (Chen et al., 2018). Schizophrenic patients have increased Rims2 levels in the brain (Weidenhofer et al., 2006; Weidenhofer et al., 2009). A loss-of-function point mutation in the Rims2 gene was the only variant risk factor for tardive dyskinesia in a recent whole-exome clinical study (Alkelai et al., 2019). Finally, polymorphisms in the Rims2 gene are associated with degenerative lumbar scoliosis (Kim et al., 2013).

Another unique feature of Rims2 neurobiology, which could have relevance germane to finding here, is its remarkably high ratio of circular RNAs (circRNAs) to linear mRNA in the human and mouse brain (20 fold higher) (Rybak-Wolf et al., 2015). Notably, circRims2 localizes primarily to the cerebellum in the adult mouse brain and is produced by "backsplicing" of pre-mRNAs which yields highly stable transcripts with long half-lifes (Holdt et al., 2018; Rybak-Wolf et al., 2015). RBPs were recently shown to play a major role in regulating circRNA expression in the brain (Ji et al., 2019). Given that: (a) RBM5 is an RBP which regulates Rims2 splicing (as shown here for the first time), (b) total Rims2 mRNA staining was markedly increased in the cerebellum, and (c) gross cerebellar morphology was altered in KOs - we speculate that RBM5 might regulate circRims2 splicing as well. Our assays were unable to investigate circRNAs but remains an important direction for future studies.

In summary, this is the first study to elucidate genes regulated by RBM5 in the intact brain. Surprisingly, RBM5 KO did not decrease the expression of pro-death genes following their induction with a CCI-TBI *in vivo*. The unexpected finding subverts our current thinking germane to the possible gene pathways regulated by RBM5 in the brain. Whereas it potently promotes the expression of cell death genes in cancer, we found that RBM5 regulates the expression and splicing of genes with a presumptive role in neurotransmission. More studies are needed to determine if blocking RBM5 *in vivo* is neuroprotective and whether it activates novel mechanisms which could have therapeutic benefits in the setting of a brain injury.

Supplementary Material

Refer to Web version on PubMed Central for supplementary material.

Acknowledgements:

We are grateful to the University of Pittsburgh Genomics Core and to The Moffitt Cancer Center Genomics Core for assistance in RNA studies. This work was supported by NIH/NINDS grants R01NS105721 to TCJ, and R01NS087978 to PMK and EKJ, by the University of South Florida Morsani College of Medicine start-up funds to TCJ, and by the Ake N. Grenvik Chair in Critical Care Medicine to PMK.

Abbreviations:

RBPs	RNA-binding proteins
RBM5	RNA-binding motif 5

RRM	RNA recognition motif
OCRE	Octamer repeat of aromatic residues
Csnka2ip/CKT2	Casein kinase 2 alpha prime interacting protein
Rims2	Regulating synaptic membrane exocytosis 2
TBI	Traumatic brain injury
CCI	Controlled cortical impact
GFAP	Glial fibrillary acidic protein
Slc20a1	Solute carrier family 20 member 1
Mef2a	Myocyte enhancer factor 2a
Ndrg2	N-Myc Downstream-Regulated Gene 2 Protein
ISH	In Situ Hybridization
PPIB	Cyclophilin B
dapB	bacillus subtilis dihydrodipicolinate reductase

References

Alkelai A, Greenbaum L, Heinzen EL, Baugh EH, Teitelbaum A, Zhu XL, Strous RD, Tatarskyy P, Zai CC, Tiwari AK, Tampakeras M, Freeman N, Muller DJ, Voineskos AN, Lieberman JA, Delaney SL, Meltzer HY, Remington G, Kennedy JL, Pulver AE, Peabody EP, Levy DL, Lerer B, 2019. New insights into tardive dyskinesia genetics: Implementation of whole-exome sequencing approach. Prog Neuro-Psychoph 94.

Ashburner M, Ball CA, Blake JA, Botstein D, Butler H, Cherry JM, Davis AP, Dolinski K, Dwight SS, Eppig JT, Harris MA, Hill DP, Issel-Tarver L, Kasarskis A, Lewis S, Matese JC, Richardson JE, Ringwald M, Rubin GM, Sherlock G, 2000. Gene ontology: tool for the unification of biology. The Gene Ontology Consortium. Nat Genet 25, 25–29. [PubMed: 10802651]

Bai XY, Silvius D, Chan ED, Escalier D, Xu SX, 2009. Identification and characterization of a novel testis-specific gene CKT2, which encodes a substrate for protein kinase CK2. Nucleic Acids Res 37, 2699–2711. [PubMed: 19273531]

Bazarian JJ, Biberthaler P, Welch RD, Lewis LM, Barzo P, Bogner-Flatz V, Gunnar Brolinson P, Buki A, Chen JY, Christenson RH, Hack D, Huff JS, Johar S, Jordan JD, Leidel BA, Lindner T, Ludington E, Okonkwo DO, Ornato J, Peacock WF, Schmidt K, Tyndall JA, Vossough A, Jagoda AS, 2018. Serum GFAP and UCH-L1 for prediction of absence of intracranial injuries on head CT (ALERT-TBI): a multicentre observational study. Lancet Neurol 17, 782–789. [PubMed: 30054151]

Bechara EG, Sebestyen E, Bernardis I, Eyras E, Valcarcel J, 2013. RBM5, 6, and 10 differentially regulate NUMB alternative splicing to control cancer cell proliferation. Mol Cell 52, 720–733. [PubMed: 24332178]

Boda E, Pini A, Hoxha E, Parolisi R, Tempia F, 2009. Selection of Reference Genes for Quantitative Real-time RT-PCR Studies in Mouse Brain. J Mol Neurosci 37, 238–253. [PubMed: 18607772]

Bonnal S, Martinez C, Forch P, Bachi A, Wilm M, Valcarcel J, 2008. RBM5/Luca-15/H37 regulates Fas alternative splice site pairing after exon definition. Mol Cell 32, 81–95. [PubMed: 18851835]

Carbon S, Douglass E, Dunn N, Good B, Harris NL, Lewis SE, Mungall CJ, Basu S, Chisholm RL, Dodson RJ, Hartline E, Fey P, Thomas PD, Albou LP, Ebert D, Kesling MJ, Mi H, Muruganujian A, Huang X, Poudel S, Mushayahama T, Hu JC, LaBonte SA, Siegele DA, Antonazzo G, Attrill H,

Brown NH, Fexova S, Garapati P, Jones TEM, Marygold SJ, Millburn GH, Rey AJ, Trovisco V, dos Santos G, Emmert DB, Falls K, Zhou P, Goodman JL, Strelets VB, Thurmond J, Courtot M, Osumi-Sutherland D, Parkinson H, Roncaglia P, Acencio ML, Kuiper M, Laegreid A, Logie C, Lovering RC, Huntley RP, Denny P, Campbell NH, Kramarz B, Acquaah V, Ahmad SH, Chen H, Rawson JH, Chibucos MC, Giglio M, Nadendla S, Tauber R, Duesbury MJ, Del-Toro N, Meldal BHM, Perfetto L, Porras P, Orchard S, Shrivastava A, Xie Z, Chang HY, Finn RD, Mitchell AL, Rawlings ND, Richardson L, Sangrador-Vegas A, Blake JA, Christie KR, Dolan ME, Drabkin HJ, Hill DP, Ni L, Sitnikov D, Harris MA, Oliver SG, Ruther-Ford K, Wood V, Hayles J, Bahler J, Lock A, Bolton ER, De Pons J, Dwinell M, Hayman GT, Lauledeerkind SJF, Shimoyama M, Tutaj M, Wang SJ, D'Eustachio P, Matthews L, Balhoff JP, Aleksander SA, Binkley G, Dunn BL, Cherry JM, Engel SR, Gondwe F, Karra K, MacPherson KA, Miyasato SR, Nash RS, Ng PC, Sheppard TK, Shrivatsav VPA, Simison M, Skrzypek MS, Weng S, Wong ED, Feuermann M, Gaudet P, Bakker E, Berardini TZ, Reiser L, Subramaniam S, Huala E, Arighi C, Auchincloss A, Axelsen K, Argoud-Puy G, Bateman A, Bely B, Blatter MC, Boutet E, Breuza L, Bridge A, Britto R, Bye-A-Jee H, Casals-Casas C, Coudert E, Estreicher A, Famiglietti L, Garmiri P, Georghiou G, Gos A, Gruaz-Gumowski N, Hatton-Ellis E, Hinz U, Hulo C, Ignatchenko A, Jungo F, Keller G, Laiho K, Lemercier P, Lieberherr D, Lussi Y, Mac-Dougall A, Magrane M, Martin MJ, Masson P, Natale DA, Hyka-Nouspikel N, Pedruzzi I, Pichler K, Poux S, Rivoire C, Rodriguez-Lopez M, Sawford T, Speretta E, Shypitsyna A, Stutz A, Sundaram S, Tognolli M, Tyagi N, Warner K, Zaru R, Wu C, Diehl AD, Chan J, Cho J, Gao S, Grove C, Harrison MC, Howe K, Lee R, Mendel J, Muller HM, Raciti D, Van Auken K, Berriman M, Stein L, Sternberg PW, Howe D, Toro S, Westerfield M, Consortium GO, 2019. The Gene Ontology Resource: 20 years and still GOing strong. Nucleic Acids Res 47, D330–D338. [PubMed: 30395331]

Castello J, Ragnauth A, Friedman E, Rebholz H, 2017. CK2-An Emerging Target for Neurological and Psychiatric Disorders. Pharmaceuticals 10.

Chelluboina B, Klopfenstein JD, Pinson DM, Wang DZ, Vemuganti R, Veeravalli KK, 2015. Matrix Metalloproteinase-12 Induces Blood-Brain Barrier Damage After Focal Cerebral Ischemia. Stroke 46, 3523–3531. [PubMed: 26534974]

Chen M, Song H, Cui J, Johnson CE, Hubler GK, DePalma RG, Gu Z, Xia W, 2018. Proteomic Profiling of Mouse Brains Exposed to Blast-Induced Mild Traumatic Brain Injury Reveals Changes in Axonal Proteins and Phosphorylated Tau. J Alzheimers Dis 66, 751–773. [PubMed: 30347620]

Clark RS, Kochanek PM, Watkins SC, Chen M, Dixon CE, Seidberg NA, Melick J, Loeffert JE, Nathaniel PD, Jin KL, Graham SH, 2000. Caspase-3 mediated neuronal death after traumatic brain injury in rats. J Neurochem 74, 740–753. [PubMed: 10646526]

de Castro MAG, Bunt G, Wouters FS, 2016. Cathepsin B launches an apoptotic exit effort upon cell death-associated disruption of lysosomes. Cell Death Discov 2.

Franz G, Beer R, Intemann D, Krajewski S, Reed JC, Engelhardt K, Pike BR, Hayes RL, Wang KK, Schmutzhard E, Kampfl A, 2002. Temporal and spatial profile of Bid cleavage after experimental traumatic brain injury. J Cereb Blood Flow Metab 22, 951–958. [PubMed: 12172380]

Fushimi K, Ray P, Kar A, Wang L, Sutherland LC, Wu JY, 2008. Up-regulation of the proapoptotic caspase 2 splicing isoform by a candidate tumor suppressor, RBM5. Proc Natl Acad Sci U S A 105, 15708–15713. [PubMed: 18840686]

Holdt LM, Kohlmaier A, Teupser D, 2018. Circular RNAs as Therapeutic Agents and Targets. Front Physiol 9.

Hook G, Jacobsen JS, Grabstein K, Kindy M, Hook V, 2015. Cathepsin B is a New Drug Target for Traumatic Brain injury Therapeutics: evidence for E64d as a Promising Lead Drug Candidate. Front Neurol 6.

Jackson TC, Dixon CE, Janesko-Feldman K, Vagni V, Kotermanski SE, Jackson EK, Kochanek PM, 2018a. Acute Physiology and Neurologic Outcomes after Brain Injury in SCOP/PHLPP1 KO Mice. Sci Rep 8, 7158. [PubMed: 29739983]

Jackson TC, Du L, Janesko-Feldman K, Vagni VA, Dezfulian C, Poloyac SM, Jackson EK, Clark RS, Kochanek PM, 2015. The nuclear splicing factor RNA binding motif 5 promotes caspase activation in human neuronal cells, and increases after traumatic brain injury in mice. J Cereb Blood Flow Metab 35, 655–666. [PubMed: 25586139]

Jackson TC, Kotermanski SE, Jackson EK, Kochanek PM, 2018b. BrainPhys(R) increases neurofilament levels in CNS cultures, and facilitates investigation of axonal damage after a mechanical stretch-injury in vitro. Exp Neurol 300, 232–246. [PubMed: 29199132]

Jackson TC, Kotermanski SE, Kochanek PM, 2017. Whole-transcriptome microarray analysis reveals regulation of Rab4 by RBM5 in neurons. Neuroscience 361, 93–107. [PubMed: 28818525]

Jamsai D, Watkins DN, O'Connor AE, Merriner DJ, Gursoy S, Bird AD, Kumar B, Miller A, Cole TJ, Jenkins BJ, O'Bryan MK, 2017. In vivo evidence that RBM5 is a tumour suppressor in the lung. Scientific Reports 7.

Ji P, Wu W, Chen S, Zheng Y, Zhou L, Zhang J, Cheng H, Yan J, Zhang S, Yang P, Zhao F, 2019. Expanded Expression Landscape and Prioritization of Circular RNAs in Mammals. Cell Rep 26, 3444–3460 e3445. [PubMed: 30893614]

Kaeser PS, Deng L, Fan M, Sudhof TC, 2012. RIM genes differentially contribute to organizing presynaptic release sites. Proc Natl Acad Sci U S A 109, 11830–11835. [PubMed: 22753485]

Kaeser PS, Deng L, Wang Y, Dulubova I, Liu X, Rizo J, Sudhof TC, 2011. RIM proteins tether Ca2+ channels to presynaptic active zones via a direct PDZ-domain interaction. Cell 144, 282–295. [PubMed: 21241895]

Kang YB, Wu ZM, Cai D, Lu BG, 2018. Evaluation of reference genes for gene expression studies in mouse and N2a cell ischemic stroke models using quantitative real-time PCR. Bmc Neurosci 19.

Kim KT, Lee JS, Lee BW, Seok H, Jeon HS, Kim JH, Chung JH, 2013. Association between regulating synaptic membrane exocytosis 2 gene polymorphisms and degenerative lumbar scoliosis. Biomed Rep 1, 619–623. [PubMed: 24648997]

Kisenge RR, Toyoda H, Kang J, Tanaka S, Yamamoto H, Azuma E, Komada Y, 2003. Expression of short-form caspase 8 correlates with decreased sensitivity to Fas-mediated apoptosis in neuroblastoma cells. Cancer Sci 94, 598–605. [PubMed: 12841868]

Kiyonaka S, Wakamori M, Miki T, Uriu Y, Nonaka M, Bito H, Beedle AM, Mori E, Hara Y, De Waard M, Kanagawa M, Itakura M, Takahashi M, Campbell KP, Mori Y, 2007. RIM1 confers sustained activity and neurotransmitter vesicle anchring to presynaptic Ca+2 channels. Nat Neurosci 10, 691–701. [PubMed: 17496890]

Kroppenstedt SN, Kern M, Thomale UW, Schneider GH, Lanksch WR, Unterberg AW, 1999. Effect of cerebral perfusion pressure on contusion volume following impact injury. J Neurosurg 90, 520–526. [PubMed: 10067922]

Liao CH, Chen BH, Chiang HS, Chen CW, Chen MF, Ke CC, Wang YY, Lin WN, Wang CC, Lin YH, 2016. Optimizing a Male Reproductive Aging Mouse Model by D-Galactose Injection. Int J Mol Sci 17.

Lion T, 2001. Current recommendations for positive controls in RT-PCR assays. Leukemia 15, 1033–1037. [PubMed: 11455970]

Liu N, Raja SM, Zazzeroni F, Metkar SS, Shah R, Zhang M, Wang Y, Bromme D, Russin WA, Lee JC, Peter ME, Froelich CJ, Franzoso G, Ashton-Rickardt PG, 2003. NF-kappaB protects from the lysosomal pathway of cell death. EMBO J 22, 5313–5322. [PubMed: 14517268]

Lotocki G, Alonso OF, Dietrich WD, Keane RW, 2004. Tumor necrosis factor receptor 1 and its signaling intermediates are recruited to lipid rafts in the traumatized brain. J Neurosci 24, 11010–11016. [PubMed: 15590916]

McClard CK, Kochukov MY, Herman I, Liu Z, Eblimit A, Moayedi Y, Ortiz-Guzman J, Colchado D, Pekarek B, Panneerselvam S, Mardon G, Arenkiel BR, 2018. POU6f1 Mediates Neuropeptide-Dependent Plasticity in the Adult Brain. J Neurosci 38, 1443–1461. [PubMed: 29305536]

McGill BE, Barve RA, Maloney SE, Strickland A, Rensing N, Wang PL, Wong M, Head R, Wozniak DF, Milbrandt J, 2018. Abnormal Microglia and Enhanced Inflammation-Related Gene Transcription in Mice with Conditional Deletion of Ctcf in Camk2a-Cre-Expressing Neurons. J Neurosci 38, 200–219. [PubMed: 29133437]

Medrano JL, Naya FJ, 2017. The transcription factor MEF2A fine-tunes gene expression in the atrial and ventricular chambers of the adult heart. J Biol Chem 292, 20975–20988. [PubMed: 29054930]

Meggio F, Pinna LA, 2003. One-thousand-and-one substrates of protein kinase CK2? FASEB J 17, 349–368. [PubMed: 12631575]

Meng Q, Zhuang Y, Ying Z, Agrawal R, Yang X, Gomez-Pinilla F, 2017. Traumatic Brain Injury Induces Genome-Wide Transcriptomic, Methylomic, and Network Perturbations in Brain and Blood Predicting Neurological Disorders. EBioMedicine 16, 184–194. [PubMed: 28174132]

Mi H, Muruganujan A, Ebert D, Huang X, Thomas PD, 2019. PANTHER version 14: more genomes, a new PANTHER GO-slim and improvements in enrichment analysis tools. Nucleic Acids Res 47, D419–D426. [PubMed: 30407594]

Mourtada-Maarabouni M, Keen J, Clark J, Cooper CS, Williams GT, 2006. Candidate tumor suppressor LUCA-15/RBM5/H37 modulates expression of apoptosis and cell cycle genes. Experimental Cell Research 312, 1745–1752. [PubMed: 16546166]

Newcomb JK, Zhao X, Pike BR, Hayes RL, 1999. Temporal profile of apoptotic-like changes in neurons and astrocytes following controlled cortical impact injury in the rat. Exp Neurol 158, 76–88. [PubMed: 10448419]

O'Bryan MK, Clark BJ, McLaughlin EA, D'Sylva RJ, O'Donnell L, Wilce JA, Sutherland J, O'Connor AE, Whittle B, Goodnow CC, Ormandy CJ, Jamsai D, 2013. RBM5 Is a Male Germ Cell Splicing Factor and Is Required for Spermatid Differentiation and Male Fertility. Plos Genetics 9.

Oh JJ, Razfar A, Delgado I, Reed FA, Malkina A, Boctor B, Slamon DJ, 2006. 3p21.3 Tumor suppressor gene H37/Luca15/RBM5 inhibits growth of human lung cancer cells through cell cycle arrest and apoptosis. Cancer Res 66, 3419–3427. [PubMed: 16585163]

Oh JJ, Taschereau EO, Koegel AK, Ginther CL, Rotow JK, Isfahani KZ, Slamon DJ, 2010. RBM5/H37 tumor suppressor, located at the lung cancer hot spot 3p21.3, alters expression of genes involved in metastasis. Lung Cancer 70, 253–262. [PubMed: 20338664]

Oh JJ, West AR, Fishbein MC, Slamon DJ, 2002. A candidate tumor suppressor gene, H37, from the human lung cancer tumor suppressor locus 3p21.3. Cancer Res 62, 3207–3213. [PubMed: 12036935]

Romero JP, Muniategui A, De Miguel FJ, Aramburu A, Montuenga L, Pio R, Rubio A, 2016. EventPointer: an effective identification of alternative splicing events using junction arrays. Bmc Genomics 17.

Rybak-Wolf A, Stottmeister C, Glazar P, Jens M, Pino N, Giusti S, Hanan M, Behm M, Bartok O, Ashwal-Fluss R, Herzog M, Schreyer L, Papavasileiou P, Ivanov A, Ohman M, Refojo D, Kadener S, Rajewsky N, 2015. Circular RNAs in the Mammalian Brain Are Highly Abundant, Conserved, and Dynamically Expressed. Mol Cell 58, 870–885. [PubMed: 25921068]

Sutherland LC, Rintala-Maki ND, White RD, Morin CD, 2005. RNA binding motif (RBM) proteins: a novel family of apoptosis modulators? J Cell Biochem 94, 5–24. [PubMed: 15514923]

Tejima E, Guo S, Murata Y, Arai K, Lok J, van Leyen K, Rosell A, Wang X, Lo EH, 2009. Neuroprotective effects of overexpressing tissue inhibitor of metalloproteinase TIMP-1. J Neurotrauma 26, 1935–1941. [PubMed: 19469687]

Wang F, Flanagan J, Su N, Wang LC, Bui S, Nielson A, Wu X, Vo HT, Ma XJ, Luo Y, 2012. RNAscope: a novel in situ RNA analysis platform for formalin-fixed, paraffin-embedded tissues. J Mol Diagn 14, 22–29. [PubMed: 22166544]

Wang Y, Sudhof TC, 2003. Genomic definition of RIM proteins: evolutionary amplification of a family of synaptic regulatory proteins. Genomics 81, 126–137. [PubMed: 12620390]

Weidenhofer J, Bowden NA, Scott RJ, Tooney PA, 2006. Altered gene expression in the amygdala in schizophrenia: up-regulation of genes located in the cytomatrix active zone. Mol Cell Neurosci 31, 243–250. [PubMed: 16236523]

Weidenhofer J, Scott RJ, Tooney PA, 2009. Investigation of the expression of genes affecting cytomatrix active zone function in the amygdala in schizophrenia: effects of antipsychotic drugs. J Psychiatr Res 43, 282–290. [PubMed: 18490030]

Zhang J, Cui Z, Feng G, Bao G, Xu G, Sun Y, Wang L, Chen J, Jin H, Liu J, Yang L, Li W, 2015. RBM5 and p53 expression after rat spinal cord injury: implications for neuronal apoptosis. Int J Biochem Cell Biol 60, 43–52. [PubMed: 25578565]

Highlights:

- *In vivo* elucidation of mRNA targets regulated by RBM5 in the brain.
- RBM5 KO increases total levels of Rims2 transcripts in the cerebellum.
- RBM5 KO increases Rims2 splicing in the cortex and in the hippocampus.
- Csnka2ip mRNA ***is*** expressed in the mammalian brain.
- RBM5 KO increases total levels of Csnka2ip mRNA in the cortex.

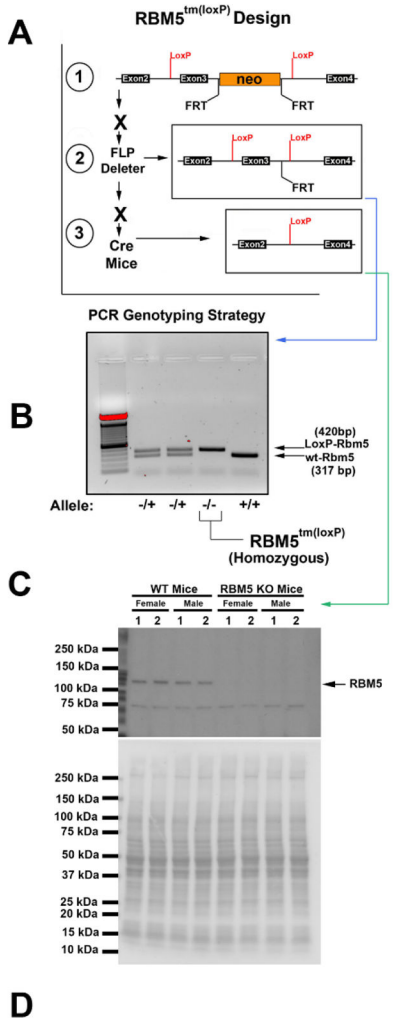

D

Fifty-Six F2 Litters (August 2017 – January 2019)				
RBM5 Genotype	**1 Copy of CRE Transgene**	**Animal Numbers**	**Expected Ratio**	***Observed Ratio**
Wild-Type Pups	Confirmed (+)	42	25%	~28%
Heterozygous Pups	Confirmed (+)	85	50%	~50%
Homozygous Pups	Confirmed (+)	23	25%	~15.3%

Fig. 1: Design Strategy of RBM5 KO Mice.

(A) Illustration of the design strategy. Exon 3 in the RBM5 gene is flanked with loxP sites. The neomycin cassette was removed prior to initiating studies by crossing novel transgenics with FLP deleters. Subsequent crossing to Nestin-CRE mice results in recombination mediated deletion of exon 3 in RBM5 and inhibition of a protein product. **(B)** PCR genotyping strategy to confirm homozygous conditional KOs. **(C)** Western blot of hippocampal extracts confirms the ~120 kDa RBM5 protein is present in WT-CRE mice but absent in homozygous KO-CRE mice. Total protein stain indicates equal loading across samples. **(D)** Mendelian ratios for brain-specific KOs in F2 litters is lower than expected.

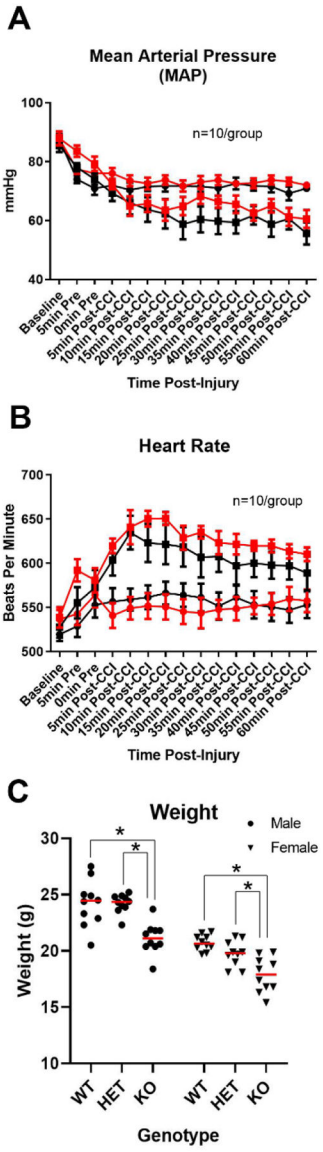

D

Blood Chemistry & Gases in WTs vs. KOs.

	Baseline (T0)	5min Pre-Injury (T1)	5min Post-CCI (T2)	60min Post-CCI (T3)	p-value
pHA	WT-S: 7.395±0.058	WT-S: 7.410±0.059	WT-S: 7.406±0.039	WT-S: 7.392±0.049	Time (T): 0.0051
	KO-S: 7.351 ±0.049	KO-S: 7.381 ±0.036	KO-S: 7.384 ±0.034	KO-S: 7.360 ±0.034	Injury (I): 0.8868
	WT-I: 7.384±0.061	WT-I: 7.401±0.034	WT-I: 7.389±0.039	WT-I: 7.401±0.046	Genotype (G):
	KO-I: 7.352±0.068	KO-I: 7.363±0.050	KO-I: 7.394±0.050	KO-I: 7.380±0.048	0.0476
PaCO2	WT-S: 33.740±5.260	WT-S: 32.110±3.191	WT-S: 33.240±2.290	WT-S: 33.690±3.883	Time: <0.0001
	KO-S: 37.250 ±5.368	KO-S: 33.890 ±3.471	KO-S: 34.190 ±3.381	KO-S: 36.130 ±2.059	Injury: 0.3773
	WT-I: 34.130±5.339	WT-I: 33.620±3.261	WT-I: 32.210±4.478	WT-I: 31.060±3.902	Genotype: 0.1986
	KO-I: 36.780±7.485	KO-I: 36.380±6.410	KO-I: 30.530±4.542	KO-I: 31.060±4.122	[T] X [I]: <0.0001
PaO2	WT-S: 170.860±30.515	WT-S: 92.460±11.743	WT-S: 81.490±17.943	WT-S: 90.120±9.857	Time: <0.0001
	KO-S: 180.000 ±21.213	KO-S: 87.750 ±6.626	KO-S: 86.990 ±7.497	KO-S: 86.260 ±6.566	Injury: 0.2397
	WT-I: 185.900±16.509	WT-I: 86.760±6.564	WT-I: 92.330±7.382	WT-I: 94.310±7.337	Genotype: 0.8396
	KO-I: 183.700±16.977	KO-I: 79.700±12.841	KO-I: 94.040±10.116	KO-I: 89.750±10.377	[T] X [I]: 0.0090
SaO2	WT-S: 98.830±2.768	WT-S: 93.510±5.444	WT-S: 89.760±13.038	WT-S: 93.760±2.907	Time: <0.0001
	KO-S: 98.720 ±0.480	KO-S: 95.520 ±3.272	KO-S: 92.100 ±2.521	KO-S: 91.650 ±2.274	Injury: 0.3462
	WT-I: 99.850±1.504	WT-I: 93.090±2.710	WT-I: 94.660±3.349	WT-I: 95.850±3.840	Genotype: 0.3214
	KO-I: 98.730±0.485	KO-I: 88.680±6.976	KO-I: 93.680±2.731	KO-I: 94.550±4.393	[T] X [I]: 0.0071
Hct	WT-S: 41.760±3.217	WT-S: 39.920±3.725	WT-S: 38.420±4.504	WT-S: 35.330±4.193	Time: <0.0001
	KO-S: 42.620 ±1.733	KO-S: 41.690 ±1.849	KO-S: 39.170 ±2.121	KO-S: 36.130 ±1.740	Injury: 0.1077
	WT-I: 42.130±1.585	WT-I: 41.290±2.466	WT-I: 37.250±3.630	WT-I: 31.400±5.409	Genotype: 0.5645
	KO-I: 43.000±1551	KO-I: 41.690±1.810	KO-I: 36.210±2.805	KO-I: 30.740±4.630	[T] X [I]: <0.0001
Hb	WT-S: 13.640±1.059	WT-S: 13.040±1.208	WT-S: 12.480±1.470	WT-S: 11.530±1.362	Time: <0.0001
	KO-S: 13.910 ±0.538	KO-S: 13.600 ±0.606	KO-S: 12.770 ±0.691	KO-S: 11.790 ±0.555	Injury: 0.1053
	WT-I: 13.730±0.533	WT-I: 13.460±0.800	WT-I: 12.170±1.180	WT-I: 10.240±1.776	Genotype: 0.5608
	KO-I: 14.040±0.499	KO-I: 13.600±0.587	KO-I: 11.840±0.914	KO-I: 10.030±1.512	[T] X [I]: <0.0001
BE	WT-S: -3.700±2.388	WT-S: -3.560±2.487	WT-S: -3.130±2.120	WT-S: -3.920±1.558	Time: 0.0001
	KO-S: -4.600±2.082	KO-S: -4.240±2.082	KO-S: -3.980±1.953	KO-S: -4.520±2.019	Injury: 0.2614
	WT-I: -4.140±2.802	WT-I: -3.230±2.381	WT-I: -4.410±2.156	WT-I: -4.770±3.174	Genotype: 0.1540
	KO-I: -4.950±1.404	KO-I: -4.350±1.255	KO-I: -5.460±1.255	KO-I: -6.060±2.151	[T] X [I]: 0.0011
HCO3	WT-S: 20.480±1.961	WT-S: 20.220±1.720	WT-S: 20.870±1.738	WT-S: 20.340±1.242	Time: 0.0001
	KO-S: 20.480 ±2.078	KO-S: 20.070 ±2.004	KO-S: 20.370 ±1.852	KO-S: 20.390 ±1.744	Injury: 0.2178
	WT-I: 20.270±2.496	WT-I: 20.880±2.300	WT-I: 19.700±2.258	WT-I: 19.300±2.857	Genotype: 0.4571
	KO-I: 20.050±1.522	KO-I: 20.460±1.914	KO-I: 18.490±1.450	KO-I: 18.280±1.971	[T] X [I]: <0.0001
Na	WT-S: 148.500±1.509	WT-S: 146.400±1.506	WT-S: 146.800±1.317	WT-S: 146.400±1.430	Time: < 0.0001
	KO-S: 149.400 ±2.011	KO-S: 147.100 ±1.912	KO-S: 147.200 ±1.398	KO-S: 147.500 ±1.900	Injury: 0.7879
	WT-I: 148.500±0.972	WT-I: 146.000±0.667	WT-I: 146.200±0.789	WT-I: 146.100±1.287	Genotype: = 0.0060
	KO-I: 150.300±1.494	KO-I: 147.900±1.853	KO-I: 147.200±1.398	KO-I: 148.000±2.000	
K+	WT-S: 4.130±0.241	WT-S: 4.300±0.275	WT-S: 4.500±0.414	WT-S: 4.540±0.430	Time: <0.0001
	KO-S: 4.080 ±0.483	KO-S: 4.500 ±0.452	KO-S: 4.480 ±0.437	KO-S: 4.560 ±0.320	Injury: 0.1096
	WT-I: 4.030±0.424	WT-I: 4.600±0.394	WT-I: 4.450±0.314	WT-I: 4.940±0.420	Genotype: 0.4559
	KO-I: 4.100±0.478	KO-I: 4.830±0.510	KO-I: 4.710±0.489	KO-I: 4.910±0.540	[T] X [I]: 0.0014
CL	WT-S: 116.200±1.989	WT-S: 117.800±2.251	WT-S: 118.300±2.541	WT-S: 119.400±2.119	Time: <0.0001
	KO-S: 117.700 ±3.129	KO-S: 118.800 ±2.616	KO-S: 120.000 ±2.708	KO-S: 120.900 ±2.885	Injury: 0.1722
	WT-I: 117.200±1.549	WT-I: 117.400±1.776	WT-I: 118.700±1.829	WT-I: 120.000±3.232	Genotype: 0.0064
	KO-I: 119.000±1.633	KO-I: 119.900±1.595	KO-I: 121.400±1.776	KO-I: 123.100±3.281	
CA	WT-S: 1.186±0.033	WT-S: 1.198±0.032	WT-S: 1.206±0.031	WT-S: 1.208±0.015	Time: 0.0004
	KO-S: 1.191 ±0.028	KO-S: 1.213 ±0.028	KO-S: 1.213 ±0.032	KO-S: 1.218 ±0.021	Injury: 0.5421
	WT-I: 1.192±0.031	WT-I: 1.208±0.029	WT-I: 1.200±0.049	WT-I: 1.178±0.042	Genotype: 0.2804
	KO-I: 1.209±0.034	KO-I: 1.220±0.023	KO-I: 1.203±0.023	KO-I: 1.182±0.018	[T] X [I]: <0.0001
Glucose	WT-S: 253.100±28.792	WT-S: 236.000±34.522	WT-S: 212.200±27.720	WT-S: 229.100±57.160	Time: 0.0056
	KO-S: 268.800±43.893	KO-S: 253.200±51.991	KO-S: 230.200±46.607	KO-S: 240.800±62.799	Injury: 0.3259
	WT-I: 218.200±39.997	WT-I: 200.400±35.362	WT-I: 206.400±41.026	WT-I: 223.000±48.208	Genotype: 0.0264
	KO-I: 250.200±19.977	KO-I: 232.000±20.971	KO-I: 257.800±17.931	KO-I: 248.200±57.896	[T] X [I]: 0.0022
Lactate	WT-S: 3.250±0.837	WT-S: 2.930±0.950	WT-S: 2.310±0.637	WT-S: 2.100±0.397	Time: <0.0001
	KO-S: 2.860 ±0.587	KO-S: 2.650 ±0.606	KO-S: 2.110 ±0.348	KO-S: 1.880 ±0.326	Injury: 0.3827
	WT-I: 3.160±0.957	WT-I: 3.060±1.752	WT-I: 2.590±0.599	WT-I: 2.520±0.744	Genotype: 0.0555
	KO-I: 2.860±0.375	KO-I: 2.360±0.395	KO-I: 2.550±0.360	KO-I: 2.120±0.210	
Osm	WT-S: 311.270±2.168	WT-S: 305.890±1.604	WT-S: 305.240±1.583	WT-S: 305.610±1.737	Time: <0.0001
	KO-S: 313.550±2.598	KO-S: 307.830±2.879	KO-S: 307.290±2.086	KO-S: 308.250±2.505	Injury: 0.8336
	WT-I: 309.310±2.615	WT-I: 303.460±2.036	WT-I: 303.970±1.747	WT-I: 308.930±3.296	Genotype: <0.0001
	KO-I: 314.720±3.200	KO-I: 308.830±3.374	KO-I: 308.930±3.296	KO-I: 309.970±2.913	[G] X [I]: 0.0387

Data Report Mean+SD Values (n=10/group; 5 males and 5 females). (I) = Injury and (S) = Sham

Fig. 2: Characterization of Acute Cardiovascular Parameters and Blood Chemistry in RBM5 KO Mice.

(**A**) KO does not alter mean arterial blood pressure (MAP) at baseline or after CCI-TBI (n=10/group). (**B**) KO does not alter heart rate (HR) at baseline or after CCI-TBI. (**C**) Body weight is decreased in male and female KOs but not in heterozygous mice. Red line depicts the mean (n=10/group). (**D**) Blood Chemistry and gas analytes in isoflurane anesthetized WT vs. KOs (n=10/group) at baseline, 5 min prior to CCI, 5 min after a CCI, and 60 min after a CCI. Graphs show mean + SEM. Black circles/squares in plots indicate WT mice. Red circles/squares in plots indicate KO mice. Data were significant at $p<0.05$. Blood chemistry variables that are significantly altered by genotype are highlighted in red text. Significant interaction terms are indicated. (I) = Injury and (S) = Sham. Arterial pH (pHA), arterial CO2 (PaCO2), arterial O2 (PaO2), arterial oxygen saturation (SaO2), hematocrit (HCt), hemoglobin (Hb), base excess (BE), bicarbonate (HCO3), sodium (Na), potassium (K), chloride (Cl), calcium (CA), osmolarity (osm).

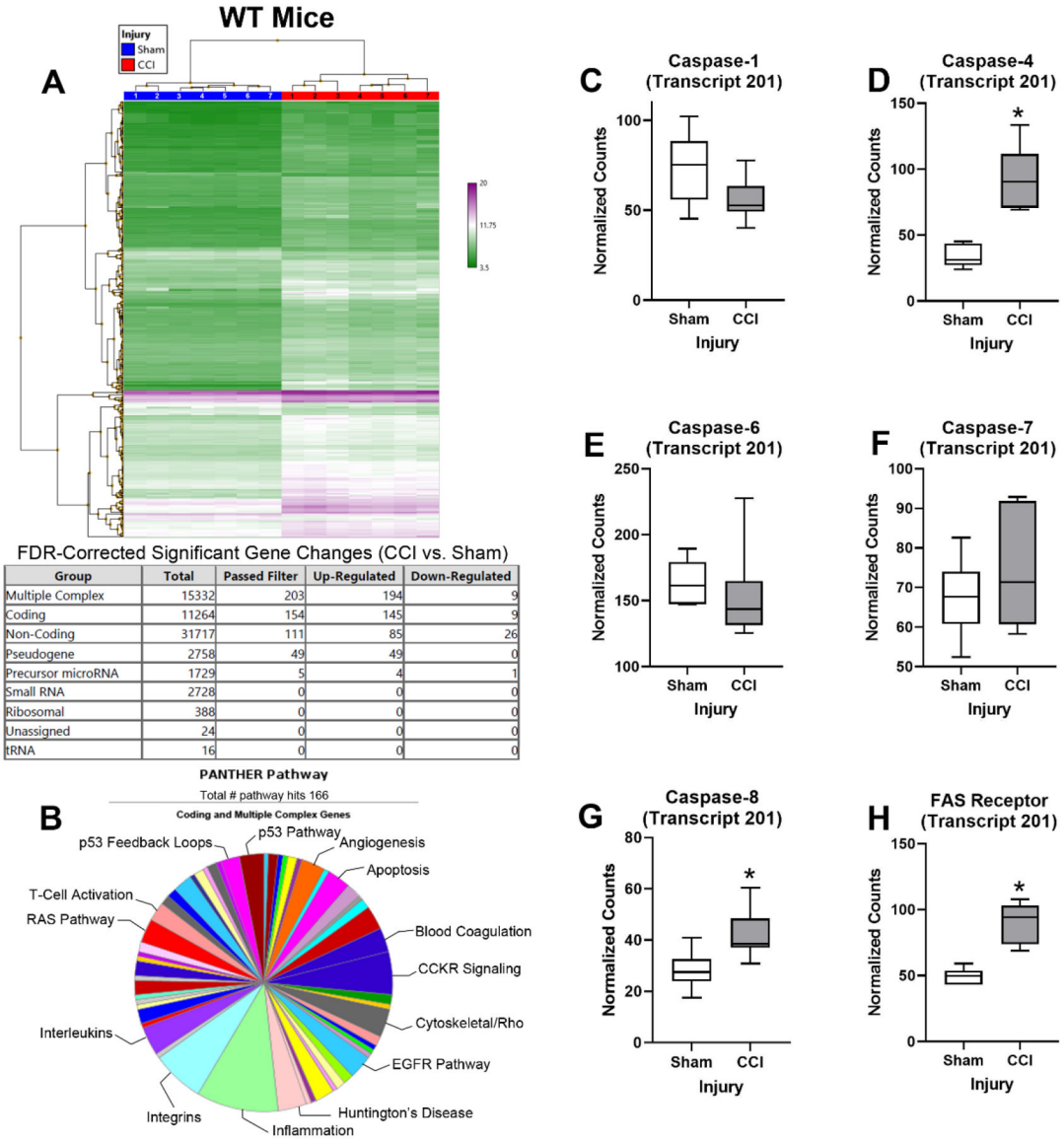

Group	Total	Passed Filter	Up-Regulated	Down-Regulated
Multiple Complex	15332	203	194	9
Coding	11264	154	145	9
Non-Coding	31717	111	85	26
Pseudogene	2758	49	49	0
Precursor microRNA	1729	5	4	1
Small RNA	2728	0	0	0
Ribosomal	388	0	0	0
Unassigned	24	0	0	0
tRNA	16	0	0	0

Fig. 3: A CCI-TBI Increases the Expression of Pro-Death Gene Targets in the Contused Cortex in WT Mice.

(A) The dendrogram shows hierarchical clustering in gene expression changes in WT shams vs. CCI-injured mice. The table below indicates the number of genes and the directionality of their change 48h post-injury. (**B**) Gene ontology of altered coding/multi-complex genes in injured WT mice. Areas of enrichment are denoted. (**C-H**) Increased levels of selected cell death gene targets in WT mice were confirmed by Nanostring quantification. Total mRNA levels of: (**D**) caspase-4, (G) caspase-8, and (H) the FAS receptor were significantly increased in the injured cortex. In contrast, levels of: (C) caspase-1, (D) caspase-6, and (F) caspase-7 did not significantly differ at the 48h endpoint in WT shams vs. CCI-injured mice. Box plots show the minimum, maximum, IQR, and median for the samples (n=7/group). Data were analyzed by a t-test and significant at $p<0.05$. Clear boxes indicate WT-Shams and grey boxes indicate WT-CCI.

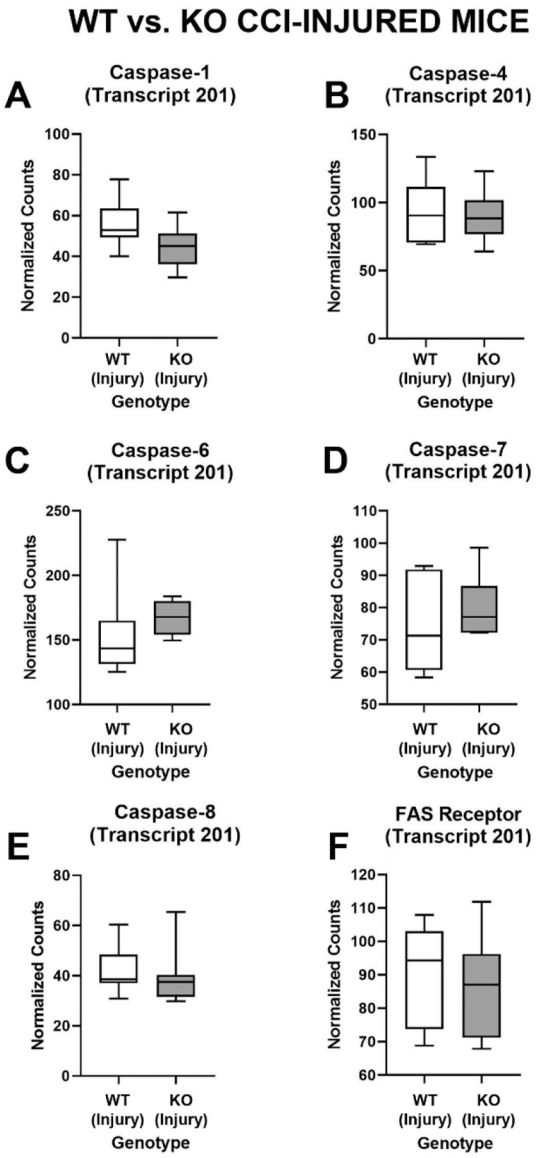

Fig. 4: RBM5 KO does not Affect the Amplitude of Pro-death Gene Expression in the Contused Cortex after a CCI-TBI.

(A) Nanostring quantification of selected cell death genes in CCI-WT vs. CCI-KO mice. Total mRNA levels of: (**A**) caspase-1, (**B**) caspase-4, (**C**) caspase-6, (**D**) caspase-7, (**E**) caspase-8, and (**F**) FAS receptor were not significantly different by genotype in the contused cortex by 48h post-injury. Box plots show the minimum, maximum, IQR, and median for the samples (n=7/group). Data were analyzed by a t-test and significant at $p<0.05$. Clear boxes indicate WT-CCI and grey boxes indicate KO-CCI. Non-significant (N.S.).

A Gene-Level Changes in RBM5 KO vs. WT Mice

GENE Symbol	ID	Sham (KO vs. WT) Fold-Change	CCI (KO vs. WT) Fold-Change	Sham (KO vs. WT) P-value (FDR)	CCI (KO vs. WT) P-value (FDR)	Gene Group
Csnka2ip	TC1600001835	2.06	2.1	7.93E-07	1.05E-06	Coding
Gm756	TC0600002811	-2.13		.0079		Coding
Serpina3n	TC1200001047	2.38		0.0260		Coding
Gfap	TC1100003856	3.12		0.0189		Multiple Complex
Gm14445	TC0200002713	-2.06		1.83E-06		Pseudogene
Gm14415	TC0200005359	-2.15		3.08E-05		Pseudogene
Gm26109	TC1800001165	-2.15		1.71E-05		Small RNA
Snord55	TC0400003364	-2.09		5.31E-05		Small RNA
Snord70	TC0100000457	-2.09		0.0001		Small RNA
----	TC0200005332	-2.23	-2.07	6.24E-10	3.34E-08	Non-Coding
----	TC0200002725	-2.06		3.68E-07		Non-Coding
----	TC0800001823	-2.06		1.89E-05		Non-Coding
----	TC1300001327	-2.01		0.0001		Non-Coding
----	TC0200002744		-2.24		1.03E-08	Non-Coding
----	TC0200005330		-2.02		1.03E-08	Non-Coding
----	TC0200005372		-2.03		1.51E-06	Non-Coding

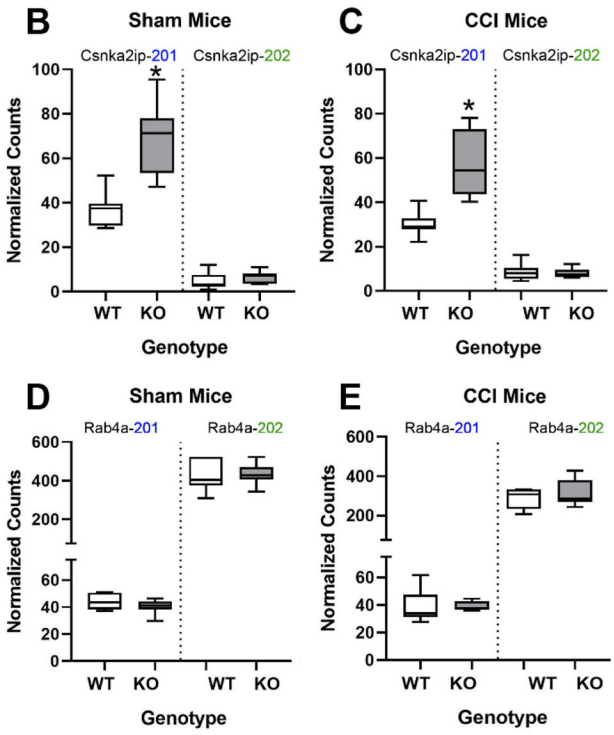

Fig. 5: Differentially Expressed Genes in the KO Cortex.

(A) The table shows the shortlist of genes that were significantly increased or decreased in KOs. Green columns compare sham-KO vs. sham-WT and show the associated FDR p-value. Orange columns compare CCI-KO vs. CCI-WT and show the associated FDR p-value. Empty blocks indicate that the gene of interest was not differentially expressed in KO vs. WT for that experimental group. The yellow column indicates the gene category. **(B)** Increased Cnska2ip-201 mRNA levels in sham-KOs was confirmed by quantitative Nanostring analysis (n=7/group). **(E)** Increased Cnska2ip-201 mRNA levels in CCI-KOs was confirmed by quantitative Nanostring analysis. (**D** and **E**) Nanostring analysis confirmed microarray findings that neither Rab4a-201 or Rab4a-202 transcripts were significantly altered in the cortex in sham-KOs or CCI-KOs vs. respective WT controls (n=7/group). Box plots show the minimum, maximum, IQR, and median for the samples

(n=7/group). Data were analyzed by a t-test and significant at $p<0.05$. Clear boxes indicate WTs and grey boxes indicate KOs.

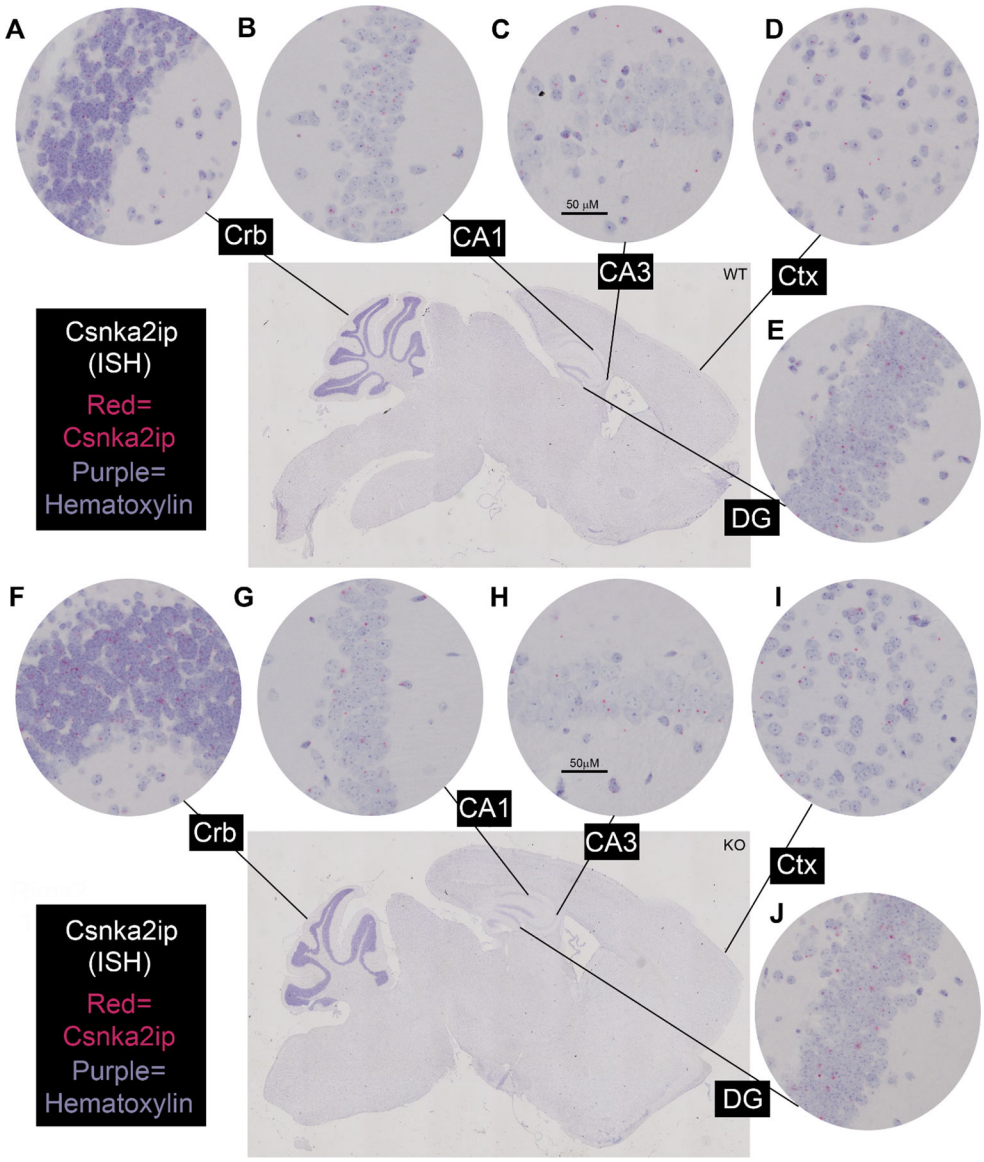

Fig. 6: Total Csnka2ip mRNA ISH Staining in the WT & KO Brain.

Sagittal brain sections were stained for Csnka2ip using RNAscope® technology. Transcripts were detected in the WT brain in the: **(A)** cerebellum, **(B)** CA1 hippocampus, **(C)** CA3 hippocampus, **(D)** cortex, and **(E)** hippocampal dentate gyrus. Csnka2ip staining was also found in the KO brain in the: **(F)** cerebellum, **(B)** CA1 hippocampus, **(C)** CA3 hippocampus, **(D)** cortex, and **(E)** hippocampal dentate gyrus. Square panels show 4X magnification of the entire stained brains. Circles show 20X magnification of sub-regions. The 20X CA3 image includes a representative scalebar (50μM distance) for reference. Hematoxylin staining is in purple. Probe-specific mRNA staining is in red.

A

Splicing Analysis in RBM5 KO vs. WT Mice

GENE Symbol	PSR	Sham (KO vs. WT) SPICING INDEX	CCI (KO vs. WT) SPICING INDEX	All KO vs. All WT SPICING INDEX	Sham (KO vs. WT) P-value (FDR)	CCI (KO vs. WT) P-value (FDR)	All KO vs. All WT P-value (FDR)	SPLICING EVENT
Mef2a	0700029383	-2.04			9.70E-11			Cassette
Phkb	0800007660	3.63	2.18	2.86	2.39E-05	0.0094	6.08E-07	Cassette
Slc20a1	0200015395	-2.42	-2.08	-2.14	1.12E-05	6.55E-05	2.39E-08	Cassette
Ndrg2	1400015119	2.34	2.03	2.29	2.48E-07	0.0076	6.98E-06	Cassette
Rims2	1500002203	5.02	5.79	5.53	1.09E-12	6.41E-13	1.59E-16	Cassette
Rims2	1500002205	3.45	3.75	3.43	2.38E-10	1.00E-10	4.76E-14	Cassette
Rims2	1500002202	3.65	3.76	3.59	3.35E-10	2.36E-10	8.78E-14	Cassette
Lrrc49	0900020445	2.07			8.37E-06			Cassette
Lrrc49	0900020419			-2.1			0.0294	Cassette
Atad2b	1200000505			2.14			5.73E-10	Cassette
Mlf2	0600011592	-2.98	-2.47	-2.71	1.61E-09	1.93E-07	6.60E-12	Intron R.
Gls	0100018618	-2.29	-2.49	-2.4	2.83E-05	1.77E-05	1.89E-08	Intron R.
Gls	0100018616		-2.01	-2.03		0.0022	1.94E-05	Intron R.
Meg3	1200008059	-2.25	-2.34	-2.32	0.0009	0.0009	1.53E-06	Intron R.
Atp13a1	0800004863	-2.06			0.0064			Intron R.
Gm14442	0200045482		-2.35	-2.16		6.51E-06	1.94E-08	Intron R.
Slc20a1	0200015397			-2.05			1.33E-06	Alt. First
Sptan 1	0200003960	-2.10	-2.06	-2.04	1.91E-05	4.56E-06	7.20E-09	Alt. First
Pnisr	0400001224	2.12	2.24	2.17	3.81E-06	1.74E-05	5.72E-09	Alt. Last
Rbfox3	1100039614	-2.39			1.42E-05			Alt. 3' A.
Rbfox3	1100039613	-2.19	-2.12	-2.2	0.0003	0.0008	8.07E-07	Alt. 3' A.
Ivns1apb	0100011187	-2.32	-2.35	-2.40	4.10E-07	1.58E-06	4.22E-10	Alt. 3' A.
Gm14411	0200045648		-2.21	-2.13		2.11E-05	3.55E-08	Complex
Nop56	0200015645		2.64	2.71		2.13E-08	1.29E-12	Complex
4933434-E20Rik				-2.01			3.33E-05	Complex

Exon 21
Exon 22
Exon 20

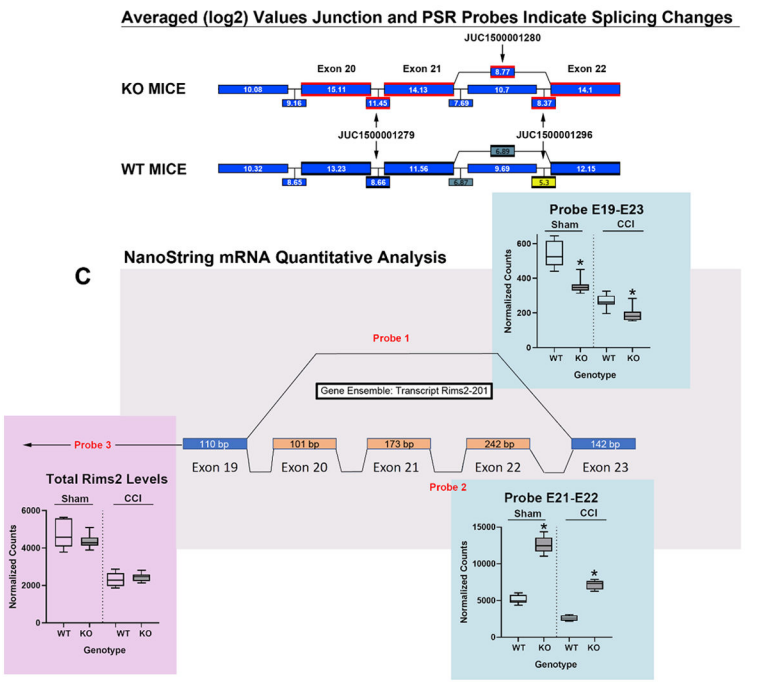

Fig. 7: Splicing Changes in the KO Cortex.

(A) The table shows the shortlist of splicing events that were significantly increased or decreased in KOs. Green columns compare sham-KO vs. sham-WT and show the associated FDR p-value. Orange columns compare CCI-KO vs. CCI-WT and show the associated FDR p-value. Blue columns show a secondary analysis of the combined datasets for sham and injured mice in each genotype (n=14/genotype). Empty blocks indicate that the splicing event for the gene of interest was not differentially expressed in KO vs. WT for that experimental group. The yellow column indicates the splicing event category. **(B)** PSR probe/junction results in TAC 4.0 software for Rims2 in KOs vs. WTs. **(C)** Altered Rims2 splicing in cortical brain samples was confirmed by quantitative Nanostring analysis. Transcripts harboring a contiguous E19-E23 spliced junction are decreased in KOs (Top blue panel). Transcripts harboring a contiguous E21-E22 spliced junction are increased in KOs (Bottom blue panel). Probes targeting a region outside of known splice sites show equivalent

levels in KOs vs. WTs (Bottom pink panel). Box plots show the minimum, maximum, IQR, and median for the samples (n=7/group). Data were analyzed by a t-test and significant at $p<0.05$. Clear boxes indicate WTs and grey boxes indicate KOs.

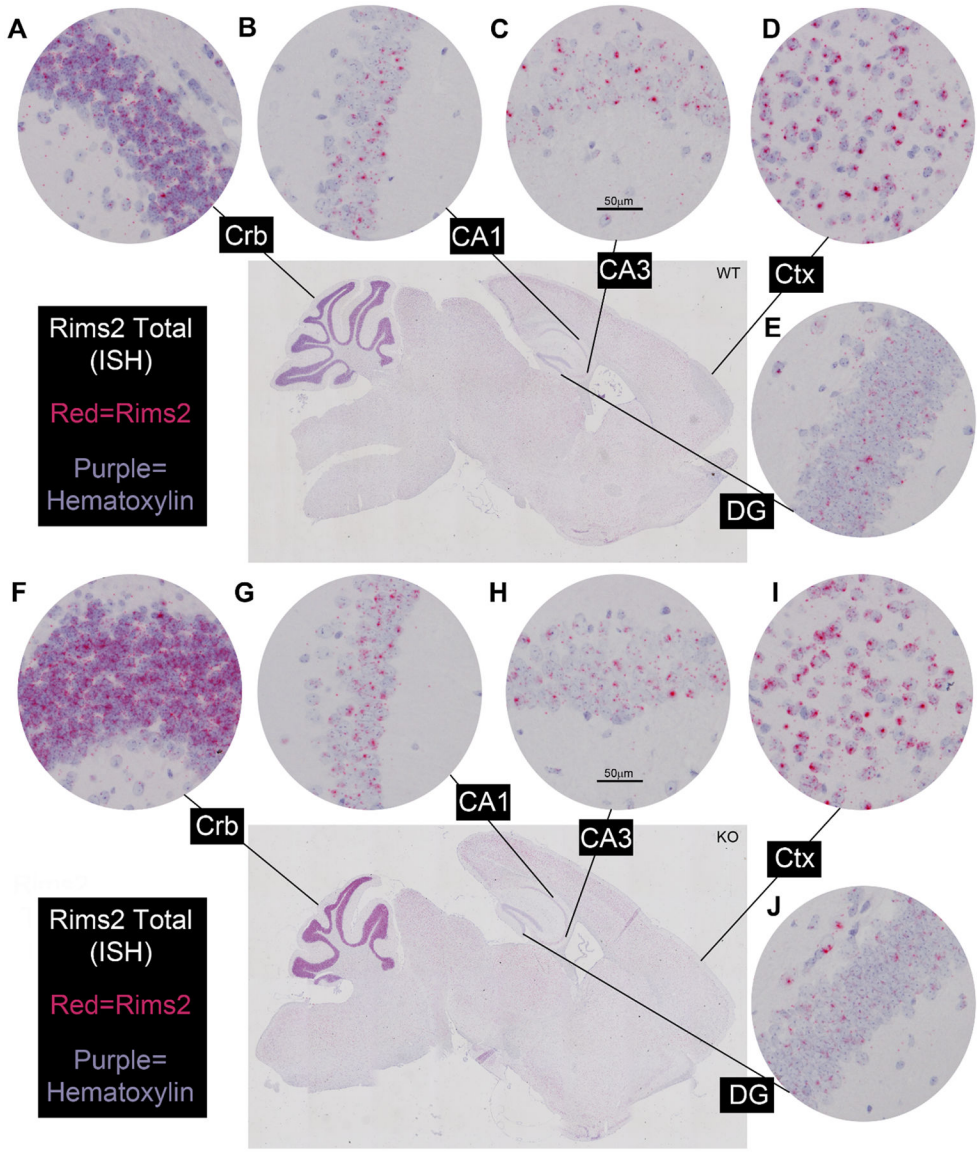

Fig. 8: Total Rims2 mRNA ISH Staining in the WT & KO Brain.

Sagittal brain sections were stained for total Rims2 mRNA using RNAscope® technology. Rims2 expression is ubiquitous in the WT brain and was seen in the: **(A)** cerebellum, **(B)** CA1 hippocampus, **(C)** CA3 hippocampus, **(D)** cortex, and **(E)** hippocampal dentate gyrus. Rims2 expression was also ubiquitous in the KO brain but levels were markedly increased in the **(F)** cerebellum. In contrast, expression in the KO: **(B)** CA1 hippocampus, **(C)** CA3 hippocampus, **(D)** cortex, and **(E)** hippocampal dentate gyrus, were compared to levels in WTs. Square panels show 4X magnification of the entire stained brains. Circles show 20X magnification of sub-regions. The 20X CA3 image includes a representative scalebar (50μM distance) for reference. Hematoxylin staining is in purple. Probe-specific mRNA staining is in red.

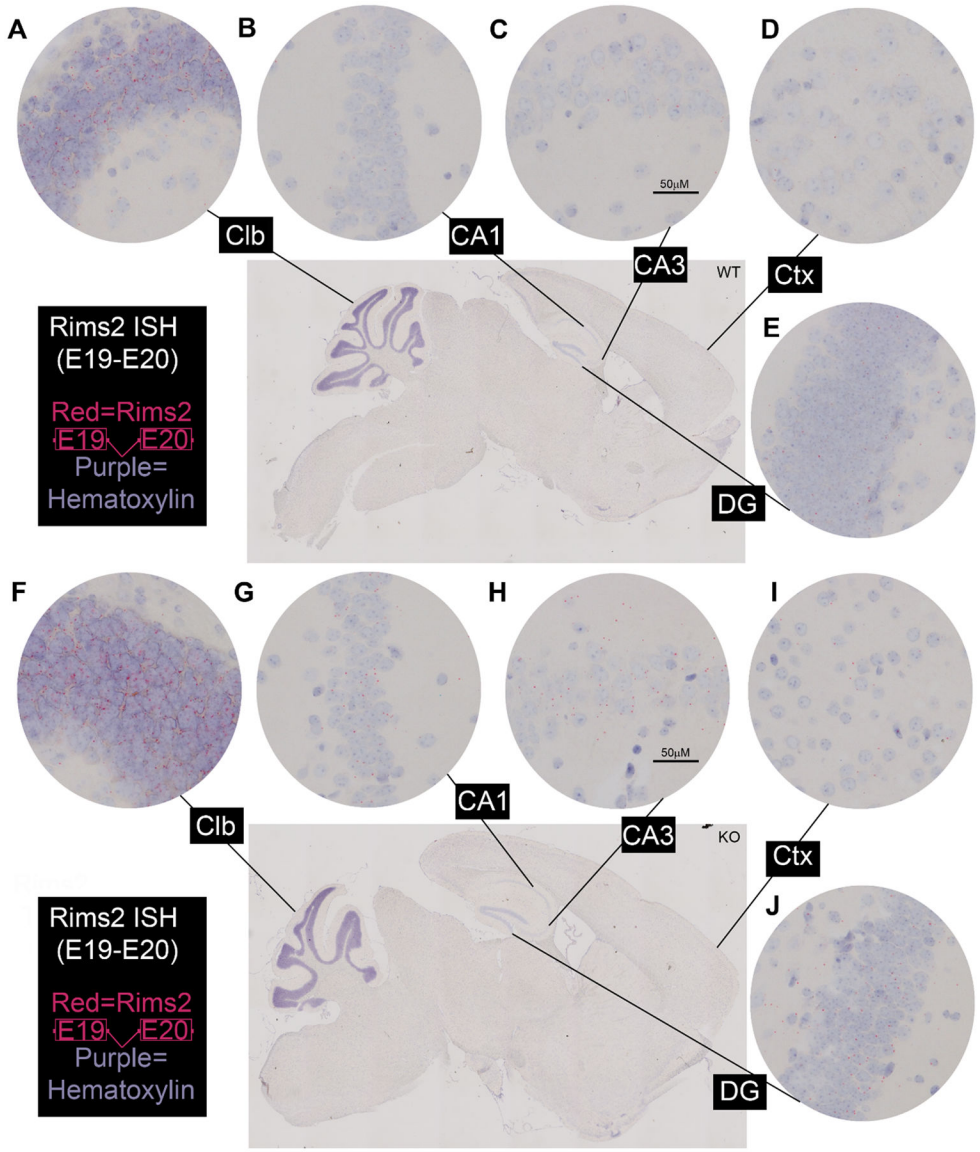

Fig. 9: Rims2 Exon Junction 19–20 ISH Staining in the WT & KO Brain.

Sagittal brain sections were stained for Rims2 splicing at the E19-E20 junction using Basescope® technology. Spliced Rims2 transcripts were detected at low levels in the WT brain in the: **(A)** cerebellum, **(B)** CA1 hippocampus, **(C)** CA3 hippocampus, **(D)** cortex, and **(E)** hippocampal dentate gyrus. Spliced Rims2 transcripts were increased in the KO: **(F)** cerebellum, **(B)** CA1 hippocampus, **(C)** CA3 hippocampus, and **(E)** hippocampal dentate gyrus. Levels were comparable to WTs in the **(D)** cortex. Square panels show 4X magnification of the entire stained brains. Circles show 20X magnification of sub-regions. The 20X CA3 image includes a representative scalebar (50μM distance) for reference. Hematoxylin staining is in purple. Probe-specific mRNA staining is in red.

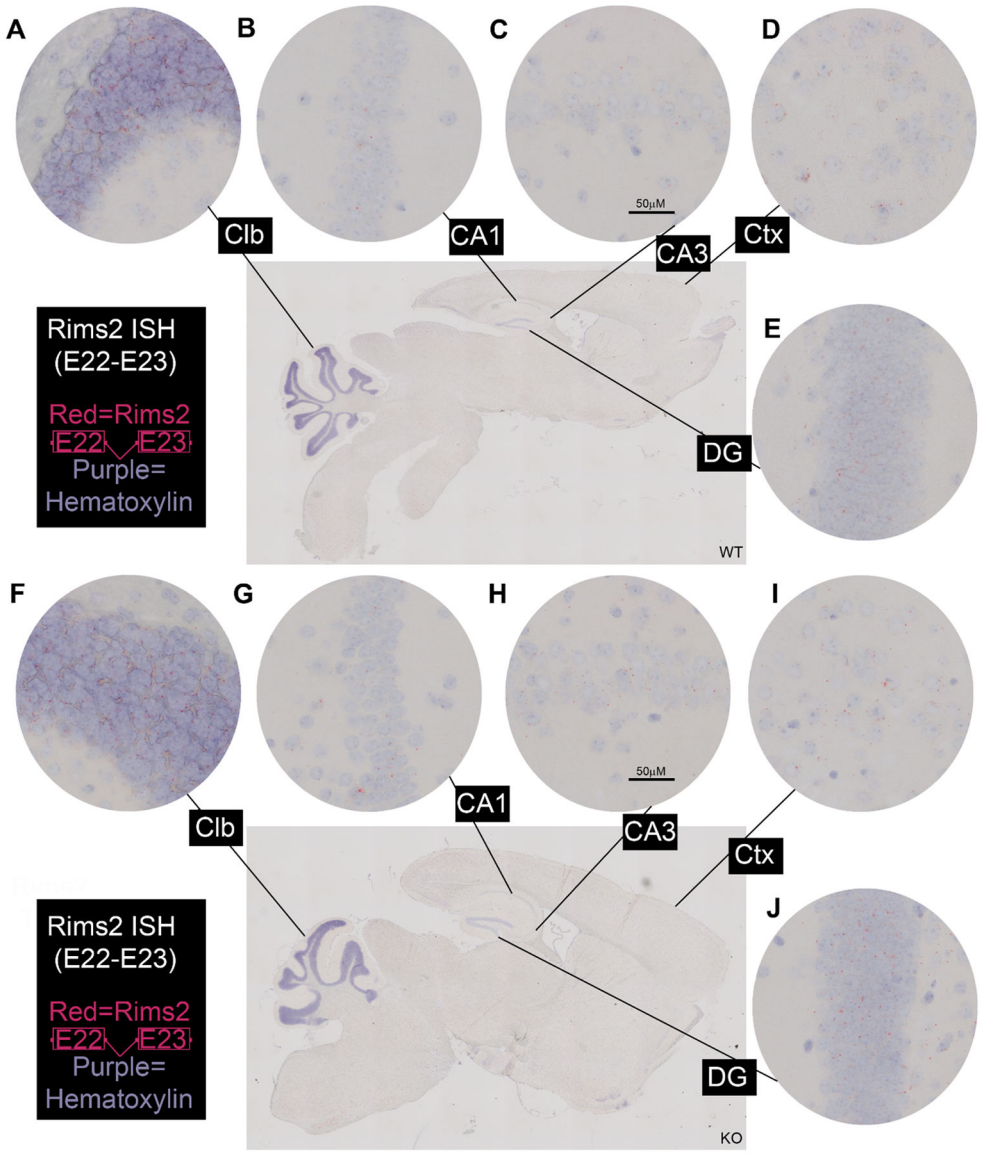

Fig. 10: Rims2 Exon Junction 22–23 ISH Staining in the WT & KO Brain.

Sagittal brain sections were stained for Rims2 splicing at the E22-E23 junction using Basescope® technology. Spliced Rims2 transcripts were detected at low levels in the WT brain in the: **(A)** cerebellum, **(B)** CA1 hippocampus, **(C)** CA3 hippocampus, **(D)** cortex, and **(E)** hippocampal dentate gyrus. Spliced Rims2 transcripts were increased in the KO brain in the: **(B)** CA1 hippocampus, **(C)** CA3 hippocampus, **(D)** cortex, and **(E)** hippocampal dentate gyrus. Levels were comparable to WTs in the **(F)** cerebellum. Square panels show 4X magnification of the entire stained brains. Circles show 20X magnification of sub-regions. The 20X CA3 image includes a representative scalebar (50μM distance) for reference. Hematoxylin staining is in purple. Probe-specific mRNA staining is in red.

Table 1: Image-J Analysis of RNAscope ISH

Target ID	Brain Region	Genotype	Averaged (3 replicates) % Area Staining	STDV	Fold Change (Ave. KO/ Ave. WT)
Total Csnka2ip	CA1 Hipp.	KO	0.590	±0.274	1.37
Total Csnka2ip	CA1 Hipp.	WT	0.431	±0.187	
Total Csnka2ip	CA3 Hipp.	KO	0.366	±0.160	0.54
Total Csnka2ip	CA3 Hipp.	WT	0.683	±0.221	
Total Csnka2ip	DG Hipp.	KO	1.025	±0.385	0.81
Total Csnka2ip	DG Hipp.	WT	1.265	±0.105	
Total Csnka2ip	Cerebellum	KO	1.696	±0.133	1.79
Total Csnka2ip	Cerebellum	WT	0.948	±0.590	
Total Csnka2ip	Cortex	KO	0.402	±0.030	1.32
Total Csnka2ip	Cortex	WT	0.304	±0.236	
Total Rims2	CA1 Hipp.	KO	4.464	±1.339	1.51
Total Rims2	CA1 Hipp.	WT	2.947	±0.516	
Total Rims2	CA3 Hipp.	KO	2.510	±0.705	0.83
Total Rims2	CA3 Hipp.	WT	3.011	±2.232	
Total Rims2	DG Hipp.	KO	1.127	±0.236	1.07
Total Rims2	DG Hipp.	WT	1.053	±0.243	
Total Rims2	Cerebellum	KO	47.681	±9.901	3.90
Total Rims2	Cerebellum	WT	12.227	±2.861	
Total Rims2	Cortex	KO	5.677	±2.646	1.57
Total Rims2	Cortex	WT	3.625	±2.263	
Total PPIB	CA1 Hipp.	KO	3.028	±0.7830	1.17
Total PPIB	CA1 Hipp.	WT	2.594	±0.7612	
Total PPIB	CA3 Hipp.	KO	16.458	±2.6595	1.41
Total PPIB	CA3 Hipp.	WT	11.666	±5.331	
Total PPIB	DG Hipp.	KO	7.898	±2.269	1.37
Total PPIB	DG Hipp.	WT	5.747	±1.972	
Total PPIB	Cerebellum	KO	0.453	±0.236	0.83
Total PPIB	Cerebellum	WT	0.544	±0.187	
Total PPIB	Cortex	KO	2.410	±2.371	1.33
Total PPIB	Cortex	WT	1.818	±0.863	

Fold Changes < -2 or > 2 are highlighted in red.

Table 2: Image-J Analysis of BaseScope ISH

Target ID	Brain Region	Genotype	Averaged (3 replicates) % Area Staining	STDV	Fold Change (Ave. KO/ Ave. WT)
Rims2 (E19-20)	CA1 Hipp.	KO	0.647	±0.111	7.80
Rims2 (E19-20)	CA1 Hipp.	WT	0.083	±0.045	
Rims2 (E19-20)	CA3 Hipp.	KO	0.575	±0.295	3.88
Rims2 (E19-20)	CA3 Hipp.	WT	0.148	±0.099	
Rims2 (E19-20)	DG Hipp.	KO	0.647	±0.109	2.46
Rims2 (E19-20)	DG Hipp.	WT	0.264	±0.117	
Rims2 (E19-20)	Cerebellum	KO	8.830	±2.967	2.72
Rims2 (E19-20)	Cerebellum	WT	3.243	±0.728	
Rims2 (E19-20)	Cortex	KO	0.497	±0.096	1.43
Rims2 (E19-20)	Cortex	WT	0.346	±0.263	
Rims2 (E22-23)	CA1 Hipp.	KO	0.222	±0.324	4.17
Rims2 (E22-23)	CA1 Hipp.	WT	0.053	±0.038	
Rims2 (E22-23)	CA3 Hipp.	KO	0.178	±0.132	3.78
Rims2 (E22-23)	CA3 Hipp.	WT	0.047	±0.005	
Rims2 (E22-23)	DG Hipp.	KO	0.287	±0.066	2.84
Rims2 (E22-23)	DG Hipp.	WT	0.101	±0.080	
Rims2 (E22-23)	Cerebellum	KO	0.485	±0.303	0.59
Rims2 (E22-23)	Cerebellum	WT	0.816	±0.582	
Rims2 (E22-23)	Cortex	KO	0.790	±0.427	4.52
Rims2 (E22-23)	Cortex	WT	0.175	±0.039	
Total PPIB	CA1 Hipp.	KO	0.944	±0.320	0.80
Total PPIB	CA1 Hipp.	WT	1.178	±0.469	
Total PPIB	CA3 Hipp.	KO	2.996	±0.246	1.13
Total PPIB	CA3 Hipp.	WT	2.662	±0.972	
Total PPIB	DG Hipp.	KO	1.837	±0.408	0.86
Total PPIB	DG Hipp.	WT	2.130	±0.383	
Total PPIB	Cerebellum	KO	0.747	±0.173	1.16
Total PPIB	Cerebellum	WT	0.644	±0.039	
Total PPIB	Cortex	KO	0.307	±0.106	0.67
Total PPIB	Cortex	WT	0.456	±0.172	

Fold Changes < -2 or > 2 are highlighted in red.

Fig. 11: Image-J Analysis of ISH Data.

(**Table 1**). The left table shows fold-change RNAscope staining levels (KO/WT) for: total Csnka2ip, total Rims2, and total PPIB (positive control). (**Table 2**): The right table shows fold-changes BaseScope staining levels (KO/WT) for: Rims2 E19-E20, Rims2 E22-E23, and total PPIB. The mean pixel staining was averaged from three regions of interest (ROIs) randomly selected within each 20X image.